AD-A078 599 MASSACHUSETTS INST OF TECH LEXINGTON LINCOLN LAB F/G 4/1
ALTAIR OBSERVATIONS OF IONOSPHERIC IRREGULARITIES AND BACKGROUN--ETC(U)
SEP 79 D M TOWLE F19628-78-C-0002
UNCLASSIFIED TN-1979-41 ESD-TR-79-223 NL

END
DATE FILMED
1-80
DDC

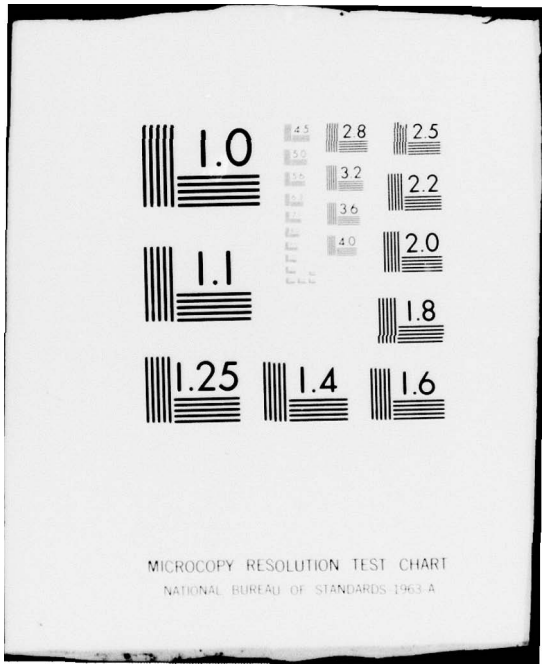
1.0
1.1
1.25
1.4
1.6
1.8
2.0
2.2
2.5
2.8
3.2
3.6
4.0
4.5
5.0
5.6
MICROCOPY RESOLUTION TEST CHART
NATIONAL BUREAU OF STANDARDS 1963 A

Technical Note 1979-41

D. M. Towle

ALTAIR Observations of Ionospheric Irregularities and Background Densities

19 September 1979

Prepared for the Defense Nuclear Agency
under Electronic Systems Division Contract F19628-78-C-0002 by

Lincoln Laboratory
MASSACHUSETTS INSTITUTE OF TECHNOLOGY
LEXINGTON, MASSACHUSETTS

The work reported in this document was performed at Lincoln Laboratory, a center for research operated by Massachusetts Institute of Technology. This work was sponsored by the Defense Nuclear Agency under Air Force Contract F19628-78-C-0002.

This technical report has been reviewed and is approved for publication.

FOR THE COMMANDER

Joseph C. Sytek

Joseph C. Sytek
Project Officer
Lincoln Laboratory Project Office

12

MASSACHUSETTS INSTITUTE OF TECHNOLOGY

LINCOLN LABORATORY

6 ALTAIR OBSERVATIONS OF IONOSPHERIC IRREGULARITIES AND BACKGROUND DENSITIES

10 David M. TOWLE
Group 37

9 TECHNICAL NOTE 1979-41

11 19 SEPTEMBER 1979

12 66

14 TN-1979-41

15 F19628-78-C-0002

LEXINGTON

16 ESD

MASSACHUSETTS

19 TR-79-223

207650

ABSTRACT

A series of measurements of the properties of equatorial ionospheric irregularities were made at Kwajalein, M.I. in August 1977 and July-August 1978. These measurements, sponsored by the Defense Nuclear Agency (DNA), involved coordinated ground based and in-situ sensors. The ARPA Long-range Tracking and Instrumentation Radar (ALTAIR), operated by Lincoln Laboratory, obtained backscatter and transmission data during five nights in August 1977 and eight nights in July-August 1978. This report describes the ALTAIR data from the night of 11 August 1978 which yield direct quantitative measurements of 1 m and 3/8 m irregularities and of plasma depleted regions. These plasma depleted regions, previously predicted on the basis of theoretical speculation and in-situ data, appear to be associated with the decay phase and not the generative phase of the field aligned irregularities.

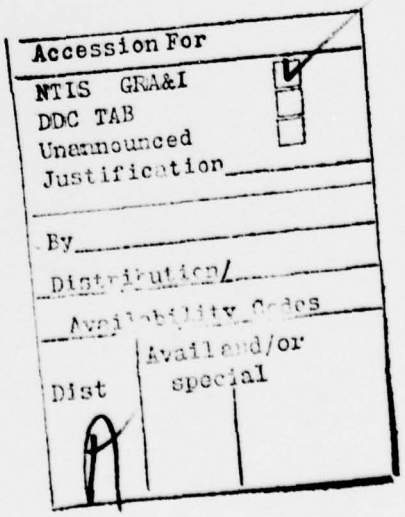

CONTENTS

I. INTRODUCTION

A campaign to obtain coordinated measurements of strong equatorial ionospheric scintillations and related generalized Spread-F ionospheric irregularities was conducted at Kwajalein, M.I. in August, 1977 and in July-August, 1978 (Greenwich Date). These measurements, sponsored by the Defense Nuclear Agency (DNA), were performed using the ground-based sensors (a large phased array ionosonde, a calibrated coherent receiver for the DNA WIDEBAND SATELLITE beacons, an optical interferometer, and the ARPA Long-range Tracking and Instrumentation Radar (ALTAIR)) as well as the rocket-borne and satellite-borne sensors of the DNA Wideband Equatorial Program (SDC-TM-1290K, March, 1978). This paper describes only selected, self-contained ALTAIR data of particular interest regarding the causes and characteristics of equatorial ionospheric irregularities.

Several types of ionospheric data were obtained by ALTAIR; namely,

1. Quasi-coherent backscatter data
2. Ionospheric propagation data
3. Incoherent backscatter data

The quasi-coherent backscatter data were gathered using the radar in two widely different waveform resolution modes, leading to macroscopic and microscopic observations of the quasi-coherent backscatter.

Strong quasi-coherent backscatter echoes were observable by ALTAIR at both the VHF (155.5 MHz) and UHF (415 MHz) frequency bands when small scale ionospheric irregularities (i.e., distributions of irregularities containing 1 m and 3/8 m sizes necessary for Bragg-type scattering at these frequencies) were illuminated by the radar when the antenna beam was oriented approximately orthogonal to the geomagnetic field lines. At Kwajalein, irregularities including these scale sizes occur frequently at nighttime, particularly during the Spring, Summer, and Autumn seasons.

Concurrent samples of coherent VHF and UHF scintillation data which document the strength, distribution, and horizontal extent of the scintillation regions were also obtained with ALTAIR by tracking selected satellites of opportunity through or above the ionospheric irregularity echo regions. Moreover, measurements of the absolute integrated electron density of the ionosphere between the radar and the satellites at successive positions along their orbits were obtained directly by measuring the group delay of the VHF pulse relative to that of the UHF pulse during the satellite tracking sessions.

The incoherent backscatter data, primarily a byproduct of the quasi-coherent measurements in these series of observations, are useful for monitoring the overall behavior of the F-region background. Additionally, on the night of 11 August 1978 the availability of an experimental waveform at UHF, capable of rapid, accurate measurements of the electron density profiles, provided detailed information on the plasma variations and depletions in the ionospheric background as well as on the development of the associated irregularities. This paper is confined to presenting the data from the night of 11 August 1978.

The experimental procedures used in acquiring the data presented in this paper and the operational parameters of ALTAIR are described. Extensive examples of the data in the form of grey scale echo region maps, signal strength sequences, and plots of electron density profiles are shown, and specific examples showing irregularity drift rates, irregularity region evolution, and density changes are discussed. The results derived from the data and the implications of these results are discussed. Correlation of the radar results with related observations from other sensors has not yet been undertaken.

II. EXPERIMENTAL PROCEDURES

Although the ALTAIR measurements are self-contained, the experimental procedures were designed to accommodate and to supplement the measurements of the other sensors used in the experiments.

A. Radar Characteristics

Table 1 lists the principal radar parameters of interest for these measurements. The characteristics which make ALTAIR particularly suited to the DNA measurement objectives are; (a) very high peak power transmitted pulses with a choice of pulse resolution widths, (b) simultaneous VHF and UHF operation, (c) a large fully steerable antenna, (d) computerized radar control, and (e) sophisticated calibration and recording systems. Fortuitously, ALTAIR is located in an equatorial region where strong ionospheric scintillations occur frequently. The operational 30 usec VHF CW pulse and both the operational 16 usec UHF CW pulse and the experimental (Mode 1B, Table 1) 40 usec UHF CW pulse were used to gather the backscatter data described in this paper.

B. Antenna Scans

To observe the momentary spatial structures of the echo regions within the field-of-view as well as their temporal development, the antenna was programmed to scan stepwise from west-to-east, repetitively. A complete scan cycle consumed about 8 min. Since the ionospheric irregularities are geomagnetically field aligned, the strongest quasi-coherent backscatter echo signals occur when the antenna main beam is oriented orthogonal to the geomagnetic field. Thus, the elevation angles during the quasi-coherent backscatter observation were normally set to point the antenna beam orthogonal to the geomagnetic field lines at a nominal altitude of 400 km. The geometry of the geomagnetic field at Kwajalein is such that when the beam is orthogonal at 400 km altitude, there is a fraction of a degree departure from

TABLE 1

ALTAIR OPERATING CHARACTERISTICS

Location:	9.5° N. Latitude (4.5° Magnetic N. Latitude)	
	167.5° E. Longitude	
Antenna:	150' Steerable Dish	
	2 Frequency Feed	
Frequency Bands:	VHF	UHF
Center Frequency (MHz)	155.5	415
Peak Power (MW)	10	20
Beam Width (deg)	2.7	1.1
Pulse Length (m)		
Mode 1A	4500	2400
Mode 1B	4500	6000 (experimental)
Mode 2	38	15

orthogonality in the E-region and in the F-region topside near 800 km; that is, near the altitude limits of interest. At VHF, these departures from orthogonality above and below 400 km during the scan result in a negligible decrease in the echo signal strength. At UHF, the misalignment, particularly at the higher altitudes, reduced the observed echo strength greatly. The directivity of the echoes at both VHF and UHF was measured to allow compensation for this effect, when necessary. However, during the transitions between adjacent beam positions, orthogonality was approximated momentarily over a wide altitude interval, yielding transient indications of the full echo strength.

During the 1978 experiments, a 25-position scan as depicted in Fig. 1 was used. (During the 11 August 1978 measurements, the first beam position was skipped.) The dwell time at each beam position was about 9 sec and the transition time between positions was about 7 sec. The scan step was designed to move the radar line-of-sight (RLOS) at the 400 km altitude level approximately 20 km longitudinally (i.e., west-to-east, magnetic longitude) between each beam position, except at the outer two positions at either end where the step distance was doubled. In terms of angular distance, the step separation was somewhat less than the VHF beamwidth of 2.7^{o}. During the return scan, three preselected central beam positions were repeated prior to initiating another scan. Provision was made in the scan control to offset the elevation angle (typically 7^{o} below geomagnetic orthogonality), particularly at these central beam positions, to aid in the observation of incoherent backscatter data which otherwise are often contaminated by the much stronger quasi-coherent backscatter signals.

The accuracy and the cross range resolution of the radar for locating features in the echo regions during the scan are determined by the antenna beamwidths. Features at adjacent beam positions were generally resolved by the UHF beam, but not by the VHF beam.

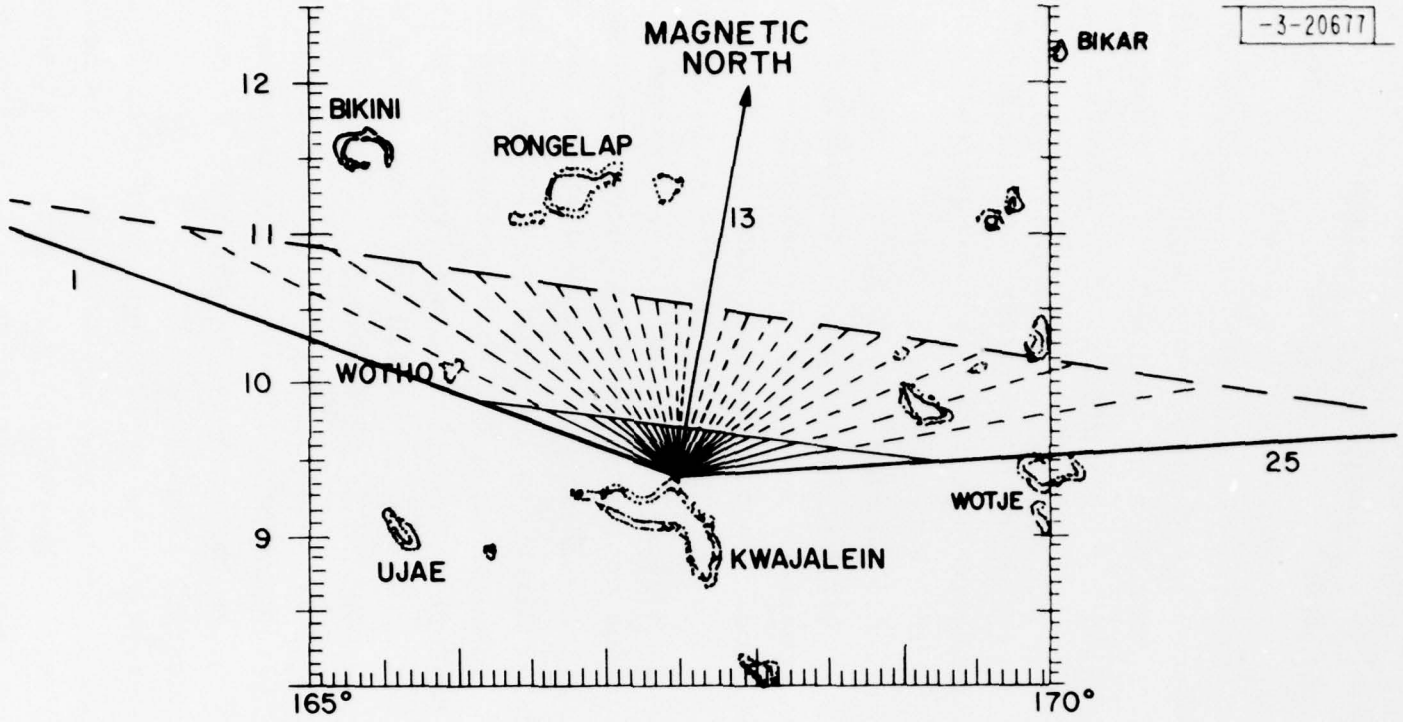

Fig. 1. ALTAIR antenna scan pattern: DNA 1978 campaign.

C. Radar Operation and Recording

Radar calibration procedures were performed prior to each scheduled evening operation. On 11 August, periods of radar silence were held from 07:45 to 08:15 and from 10:33 to 11:30 GMT to avoid RFI problems with other measurements. (Kwajalein Standard Time (KST) is GMT -12 hours. True local time is KST + 40 min.) Periodic scans were scheduled after 08:15 GMT as often as every 8 min when ionospheric activity warranted; otherwise, every half-hour or so. One satellite was tracked during the middle of the session to obtain concurrent scintillation data and to determine the integrated electron density of the ionosphere.

The data were recorded on magnetic tape, A-scope films, Range-Time-Intensity (RTI) films, and paper strip charts. Two types of magnetic recording systems were used: the regular ALTAIR Recording System (ARS) and a CDC 6600 computer controlled data recording system. Most of the data presented in this paper were recorded by the latter system. Each data record from this system comprises 330 samples of a 20 pulse signal average, plus elevation angle, azimuth angle, starting range, and time tags. VHF and UHF records assembled from interleaved pulses were recorded every second. The recording window normally extended between 90 and 830 km range with samples at 2.25 km intervals. Recordings with range resolution as fine as 15 m were made with the ARS system.

III. EXPERIMENTAL RESULTS

The VHF quasi-coherent backscatter data are displayed first in the form of grey scale maps, derived from the recorded echo signals. These maps show the general geometry and dynamics of east-west slices of the echo regions. The echo maps treat the geomagnetic orthogonality observation surface as a plane in Cartesian coordinates. The ordinate is altitude and the abscissa is east-west horizontal distance with the radar located at (0, 0). The rate of drift and the rate of development of the echo regions can be readily deduced from these maps by comparing the positions of similar echoes on successive antenna scans. This method appears to be more reliable than Doppler measurements, which tend to lump the two rates together. Sequences of plots of the video signals averaged over 2 sec intervals versus altitude and time at each beam position for several of the scans are shown also. These plots display the echo strengths and gradients more quantitatively than the grey scale maps.

The UHF data are displayed similarly. The additional sensitivity of the special UHF pulse allows the contributions of the incoherent backscatter echoes in addition to the quasi-coherent backscatter to be shown in these displays. For completeness, quantitative electron density profiles derived from the UHF data, and samples of the VHF and UHF scintillation signals associated with an observed backscatter region are presented also.

A. VHF Data

A preliminary observation at 07:40 GMT showed no irregularity echoes in the F-region. (Sporadic E-region irregularities which are present a majority of the time at Kwajalein, typically in the altitude region between 90 and 120 km were present at that time.) Figure 2 presents a grey scale map of the VHF echoes in the F-region first observed during a scan starting at about 08:19:38 GMT. In Fig. 2, the plume observed northeast of the

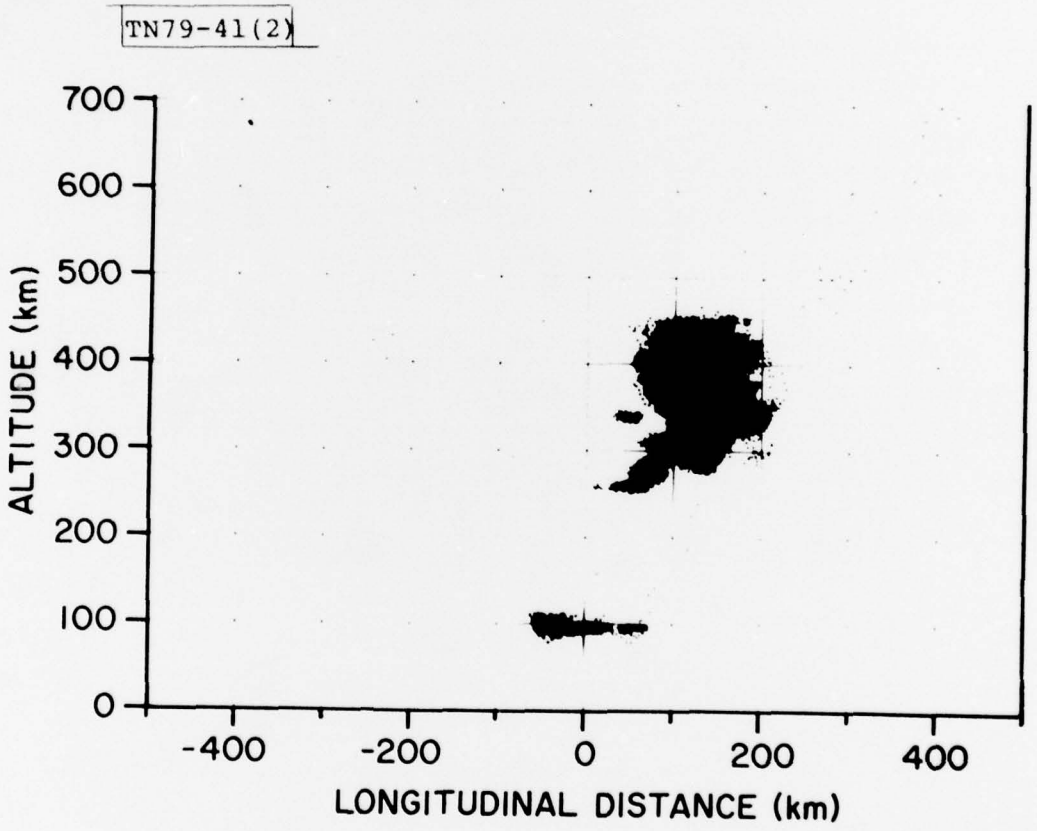

Fig. 2. VHF echo map for 08:19:38 GMT scan.

radar is apparently newly formed, but already extends well into the F-region from 250 to 450 km. Thirteen minutes later, the plume, shown in Fig. 3, had expanded upward at a rate of 95 m/sec to a height of 525 km and drifted eastward at about 90 m/sec. Twenty-five minutes later, as shown in Fig. 4, the plume was still drifting eastward at a rate of 90 m/sec and expanding upward at 95 m/sec; the top of the strong echo region reaching nearly 700 km altitude. By this time, a thinner layer of irregularities, about 30 km in altitude extent, had developed along the bottomside of the F-region. (Bottomside is defined in this paper as the lower boundary at which the ionospheric density is an order of magnitude below peak density. This is approximately the region of steepest gradient and is approximately 100 km below the peak density altitude after sunset.) This layer expanded from east-to-west approximately 300 km during the 28 min interval since the previous scan. Figure 4 shows quantitative details of the signal strength data from the 08:58:01 GMT scan. The signal strength in this plot is in dB above the peak system noise background. The RMS system noise output level for the 30 usec VHF pulse is 40LOG(R/3750) dBsm, where R is the sample range in km. The threshold for the VHF signal plots was set 3 dB above this level. The VHF incoherent backscatter signals in the middle of the F-region were usually 2 to 4 dB below the RMS noise background. Peak VHF quasi-coherent echoes up to about 43 dB above the system noise background or up to about 45 to 47 dB above the incoherent backscatter echoes were frequently observed.

Figure 5 shows that by 09:39:32 GMT, the plume observed earlier had drifted beyond the field-of-view of the radar. During the interim, the bottomside irregularity layer expanded generally upward into the middle of the F-region. Figure 5 shows that the peak VHF echo strength was a few dB stronger than during the previous scan.

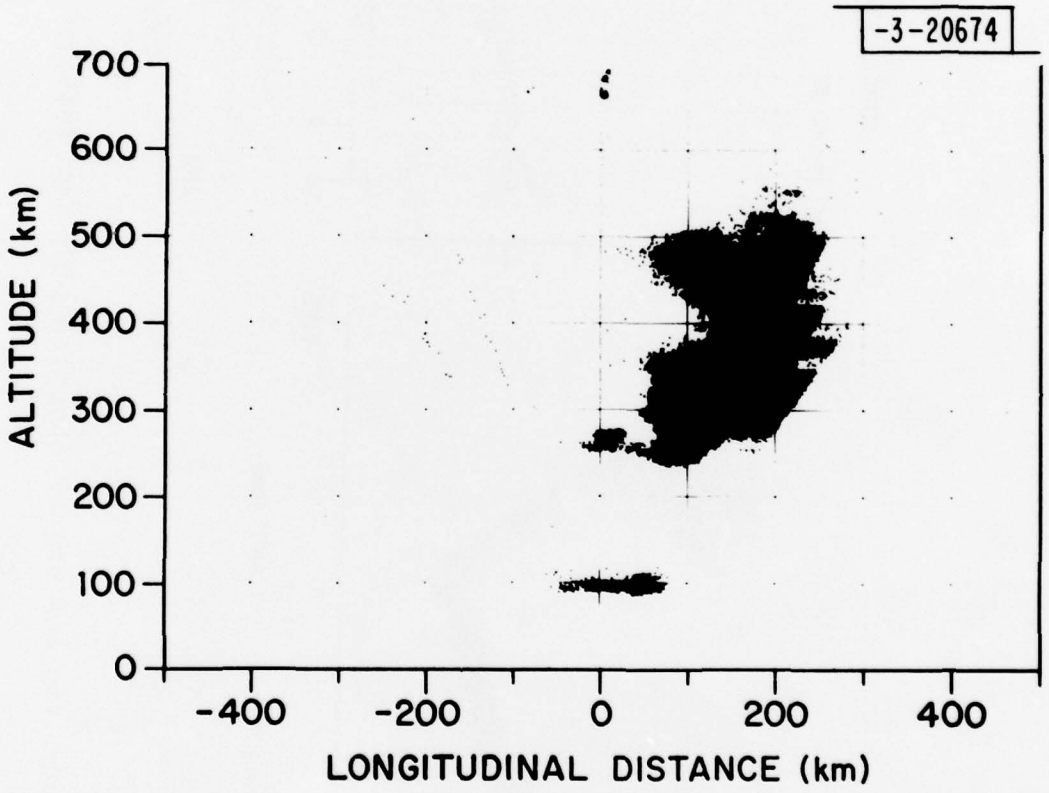

Fig. 3. VHF echo map for 08:32:39 GMT scan.

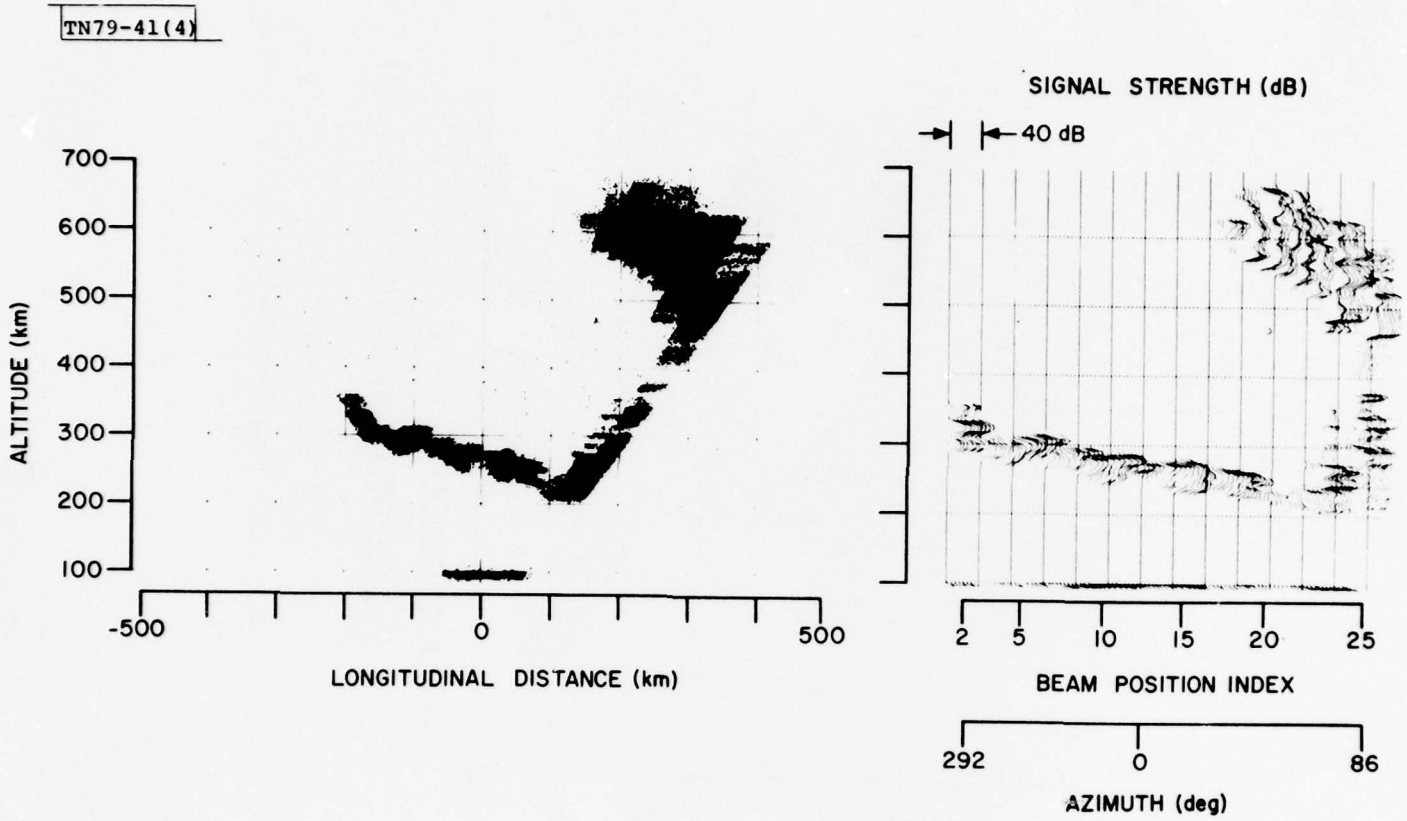

Fig. 4. VHF echo map and signal strength plot for 08:58:01 GMT scan.

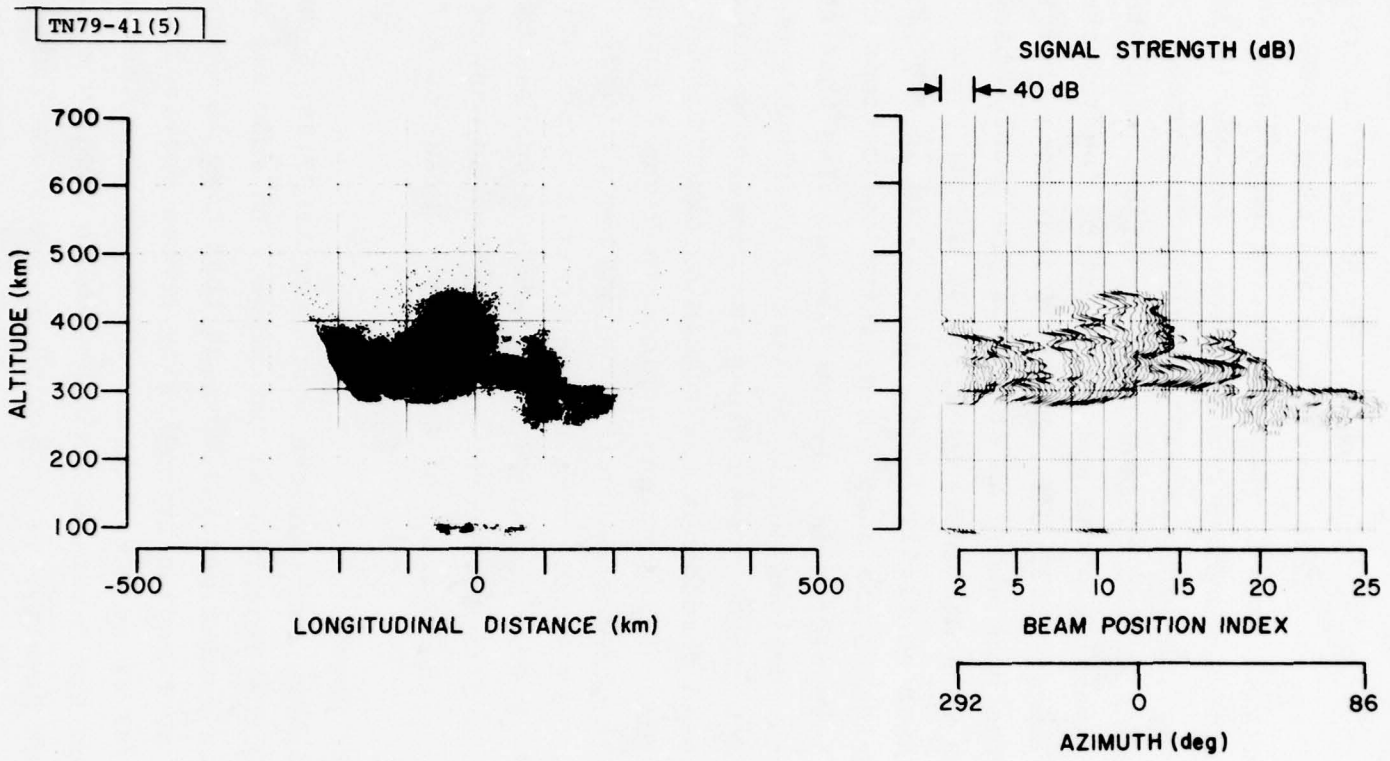

Fig. 5. VHF echo map and signal strength plot for 09:39:32 GMT scan.

The scan in which the data shown in Fig. 6 were obtained started at 11:31:31 GMT, or nearly two hours after the scan for the data in Fig. 5. Echo development was slow from 09:40 GMT until at least 10:30 GMT, when an hour of RF silence was started for purposes of arming the probe rocket. Between 10:30 and 11:30 GMT, two topside plume-like regions developed. The behavior of these plumes during subsequent observations indicate that the end of the expansive phase and the start of the dispersive phase occurred at about 11:31 GMT. Figure 6 indicates that the peak echo strengths were about as strong as previously observed, but their widths were declining by 11:31:31 GMT.

Data taken at 11:41:47 GMT, illustrated in Fig. 7, show continued drift to the east and definite indications of dispersal of the 1 m irregularities. Figure 7 shows also that the peak echo strength remained nearly as high as previously observed, but that the width of the echo regions was decreasing rapidly. This trend continued throughout the remaining observations as indicated by the maps and signal strength plots in Figs. 8 through 10, which show the VHF data acquired during the 11:56:52, 12:19:06, and 12:24:28 GMT scans. The backscattering irregularities in the radar field-of-view had almost completely dispersed by 12:30 GMT. The peak echo signal strength remained high in many of the regions until the altitude extent of the regions shrank to a few tens of kilometers.

B. UHF Data

Preliminary observations were made at 07:40:18 GMT while calibrating the experimental UHF pulse. An echo map derived from the UHF data from a partial scan at that time is shown in Fig. 11. There were no F-region irregularity echoes observed at that time, either at VHF or at UHF, but the incoherent backscatter echo signals from the F-region ionosphere were clearly evident at UHF. The F-region density, as indicated by the incoherent backscatter echoes in Fig. 11, was homogenous but with a pronounced tilt (upward from west-to-east) of the bottomside.

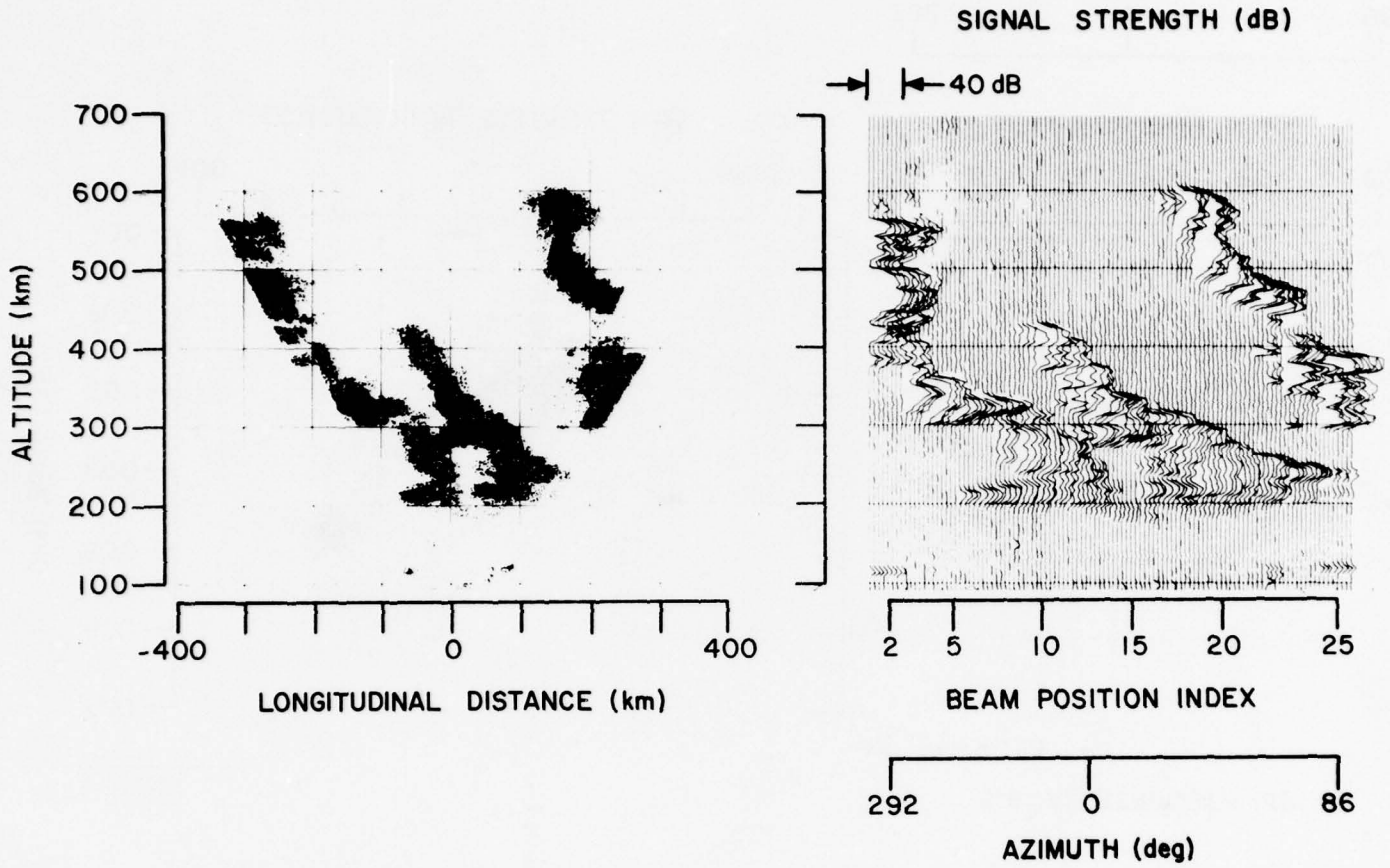

Fig. 6. VHF echo map and signal strength plot for 11:31:31 GMT scan.

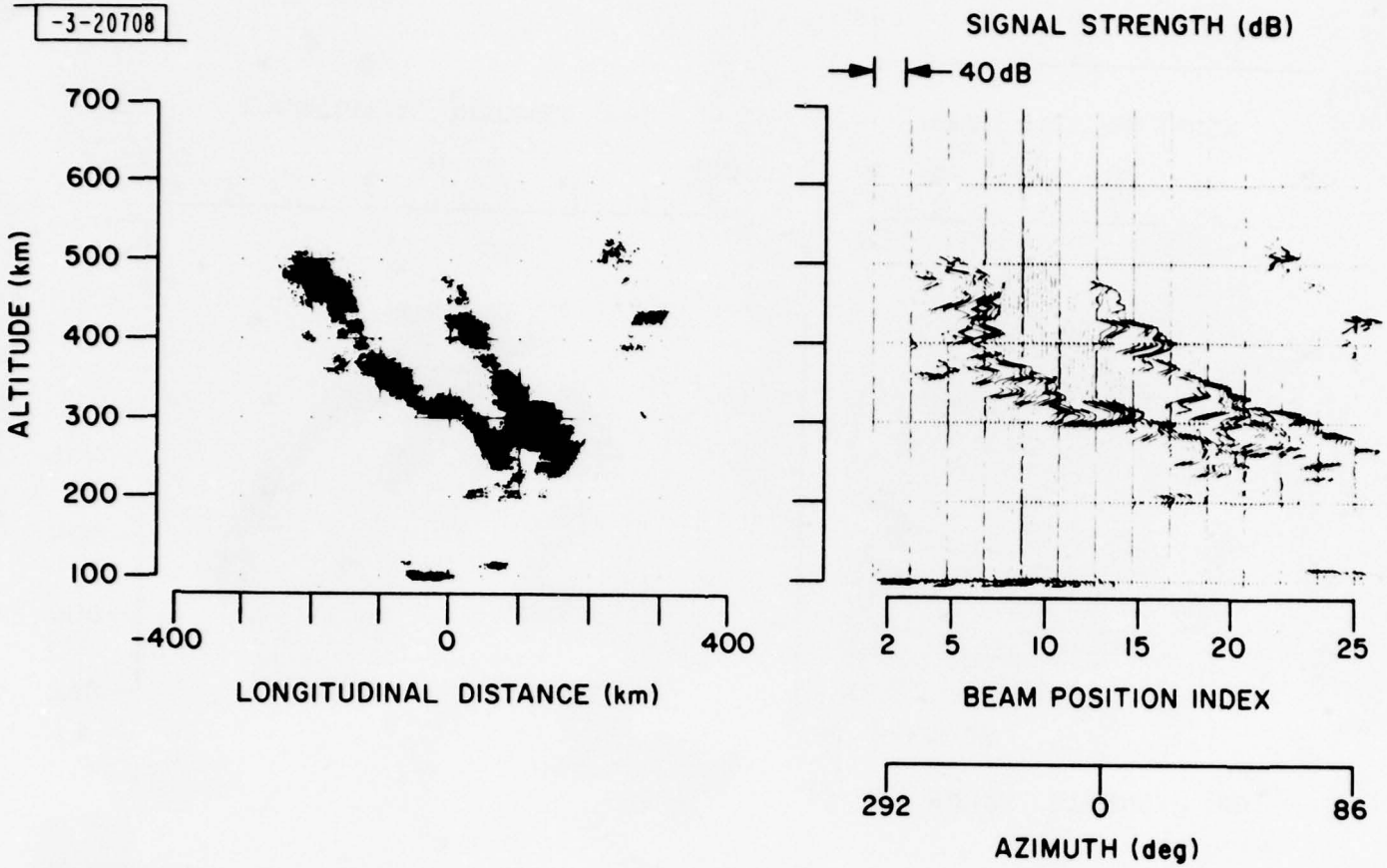

Fig. 7. VHF echo map and signal strength plot for 11:41:47 GMT scan.

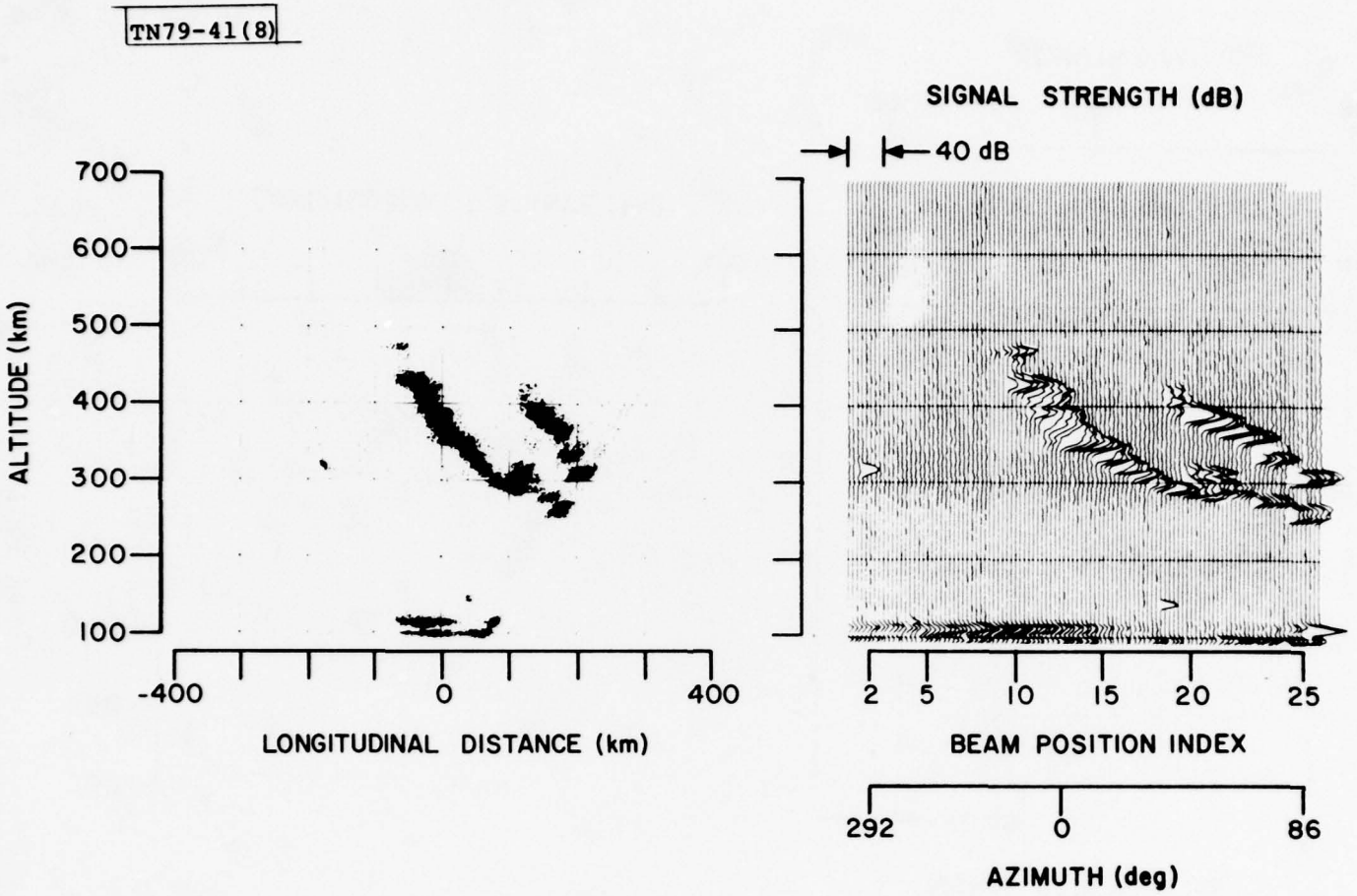

Fig. 8. VHF echo map and signal strength plot for 11:56:52 GMT scan.

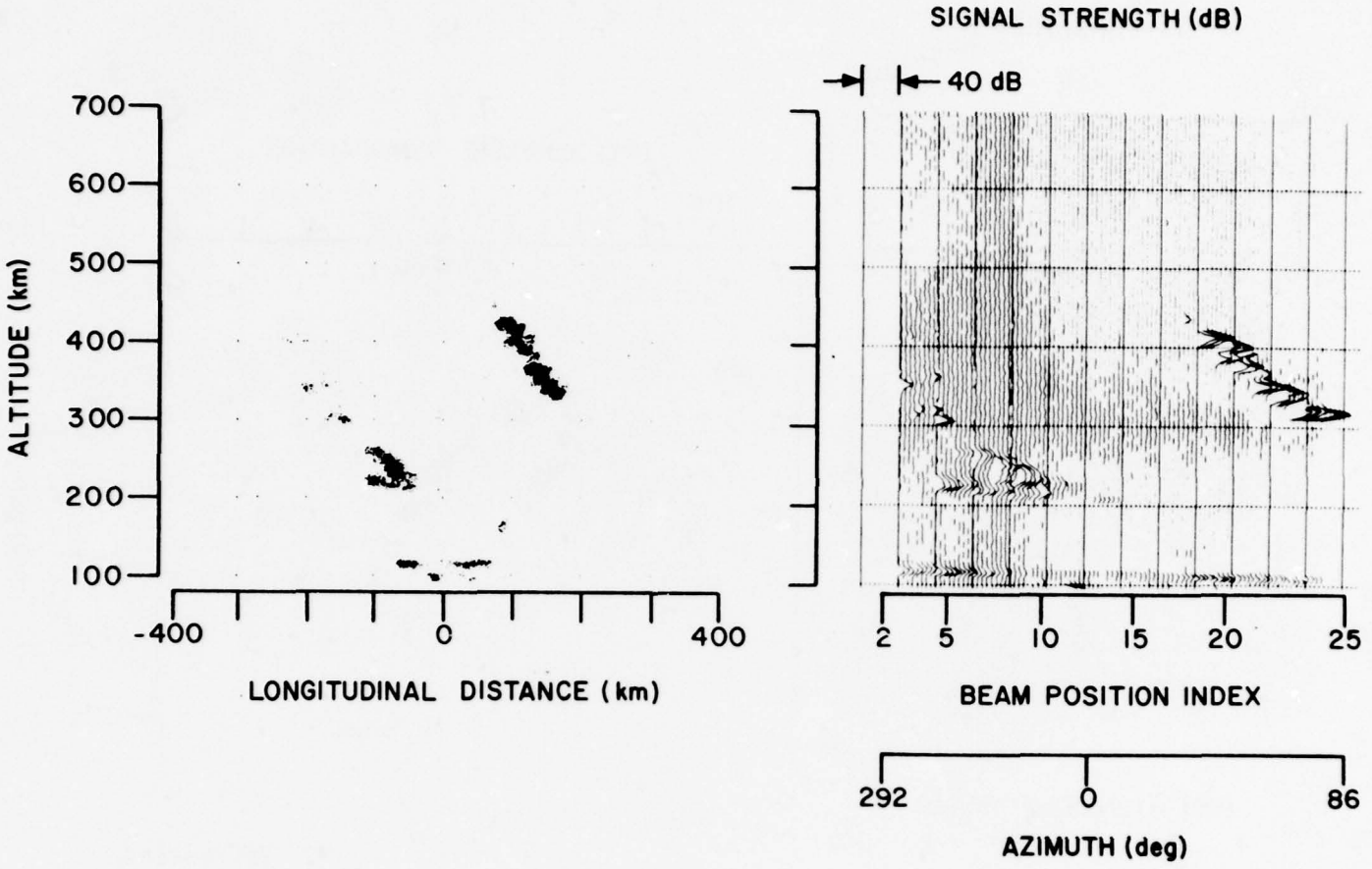

Fig. 9. VHF echo map and signal strength plot for 12:19:06 GMT scan.

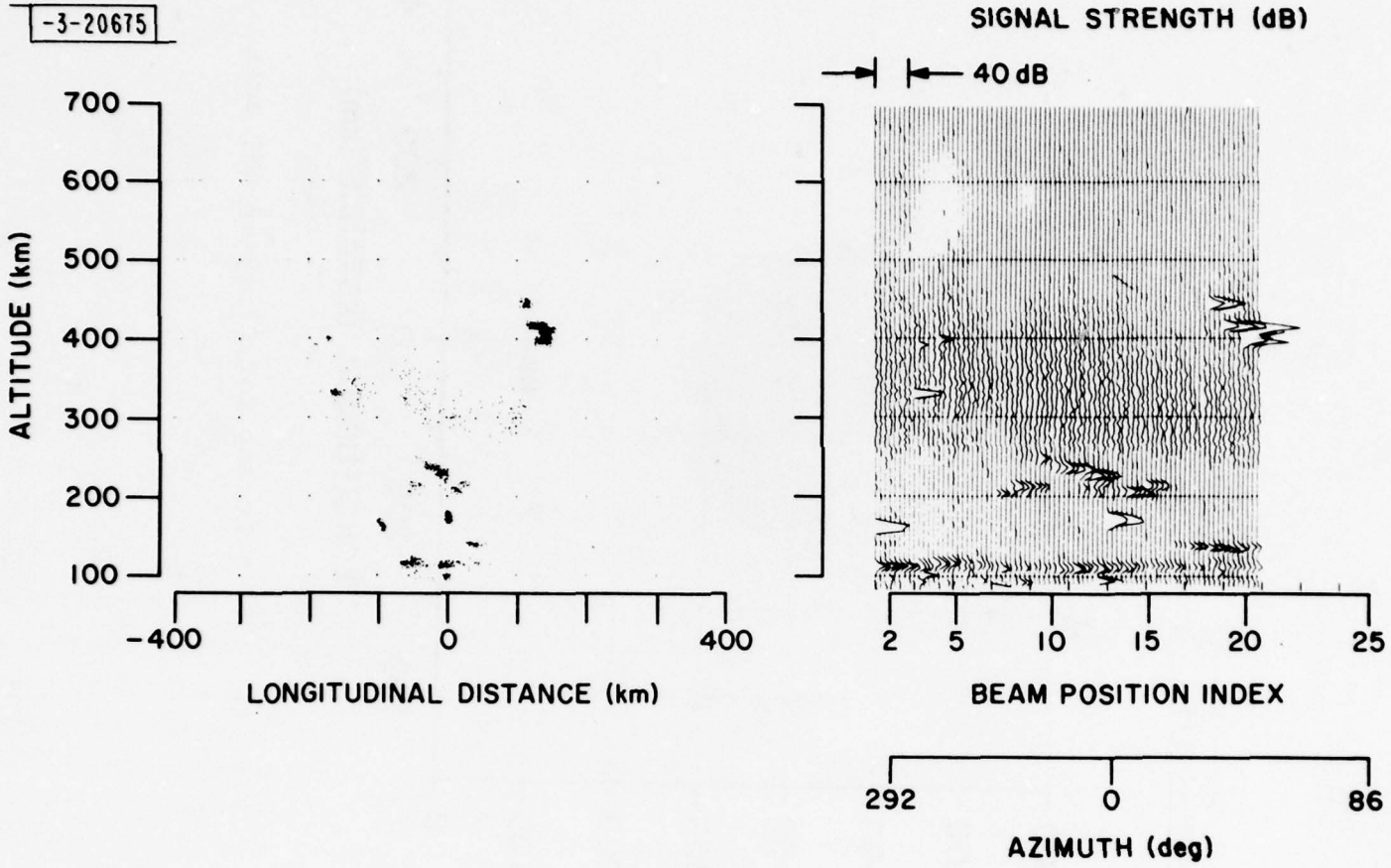

Fig. 10. VHF echo map and signal strength plot for 12:24:28 GMT scan.

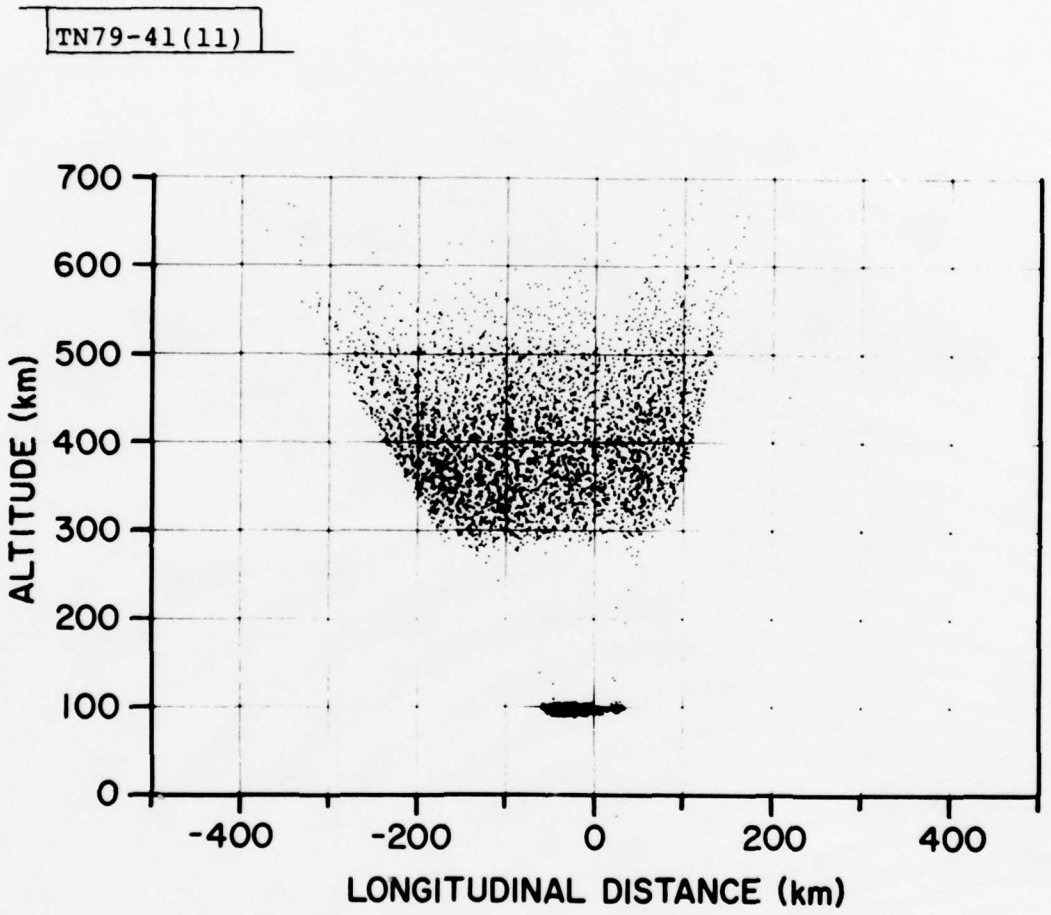

Fig. 11. UHF echo map for 07:40:18 GMT scan.

During the first of the regularly scheduled antenna scans, starting at 08:19:38 GMT, UHF echoes were observed using the normal 16 usec UHF pulse, as shown in Fig. 12, in the same region where VHF echoes (Fig. 2) were observed at that time. During the scan starting at 08:58:01 GMT, strong UHF irregularity echoes were observed with the 40 usec UHF pulse (Fig. 13) along the bottomside of the F-region. These UHF observations are similar to the VHF observations except for the greater resolution of the UHF beam. On the topside, between 450 and 650 km altitude in the northeast sector, strong UHF echoes were received only transiently, since the antenna beam passed quickly through the orthogonality position at high altitudes while proceeding to the orthogonality position for the middle F-region. Because of the greater sensitivity of the long UHF pulse, Fig. 13 clearly shows the incoherent backscatter F-region background echoes. The upward east-to-west tilt of the F-region bottomside is nearly reversed from its condition 80 min earlier (Fig. 11). The UHF echo signal strength for this scan is also shown quantitatively in Fig. 13. The UHF signal strength displayed is in dB referenced to the background system output noise level, which is 40LOG(R/5650) dBsm, where R is the sample range. In the middle of the F-region, the incoherent echo signal was approximately equal to the system noise level for the 40 usec UHF pulse.

Figure 14 shows the UHF echo map and the UHF signal strength plot for the scan starting at 09:39:32 GMT, where the irregularities have spread along the bottomside and have expanded up into the middle of the F-region. For this situation, the UHF echoes (Fig. 14) were especially strong and are strikingly similar to the VHF results (Fig. 5) for the same scan. Plots of the echo regions and the echo signal strength for the UHF scan starting at 11:31:31 GMT are shown in Fig. 15. The UHF echoes were also similar to the VHF echoes at that time. The transient orthogonality

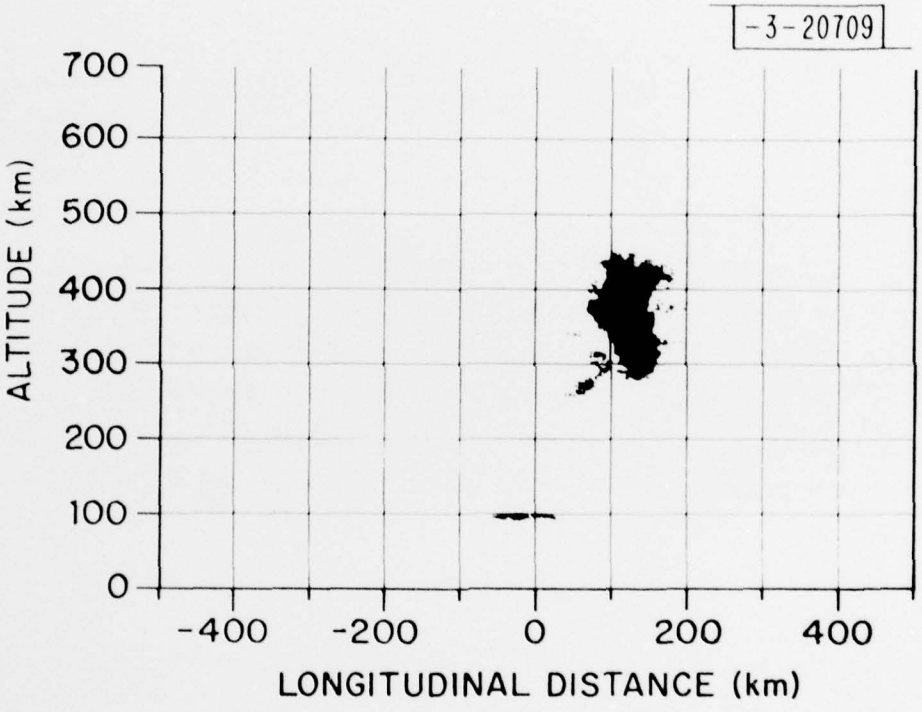

Fig. 12. UHF echo map for 08:19:38 GMT scan.

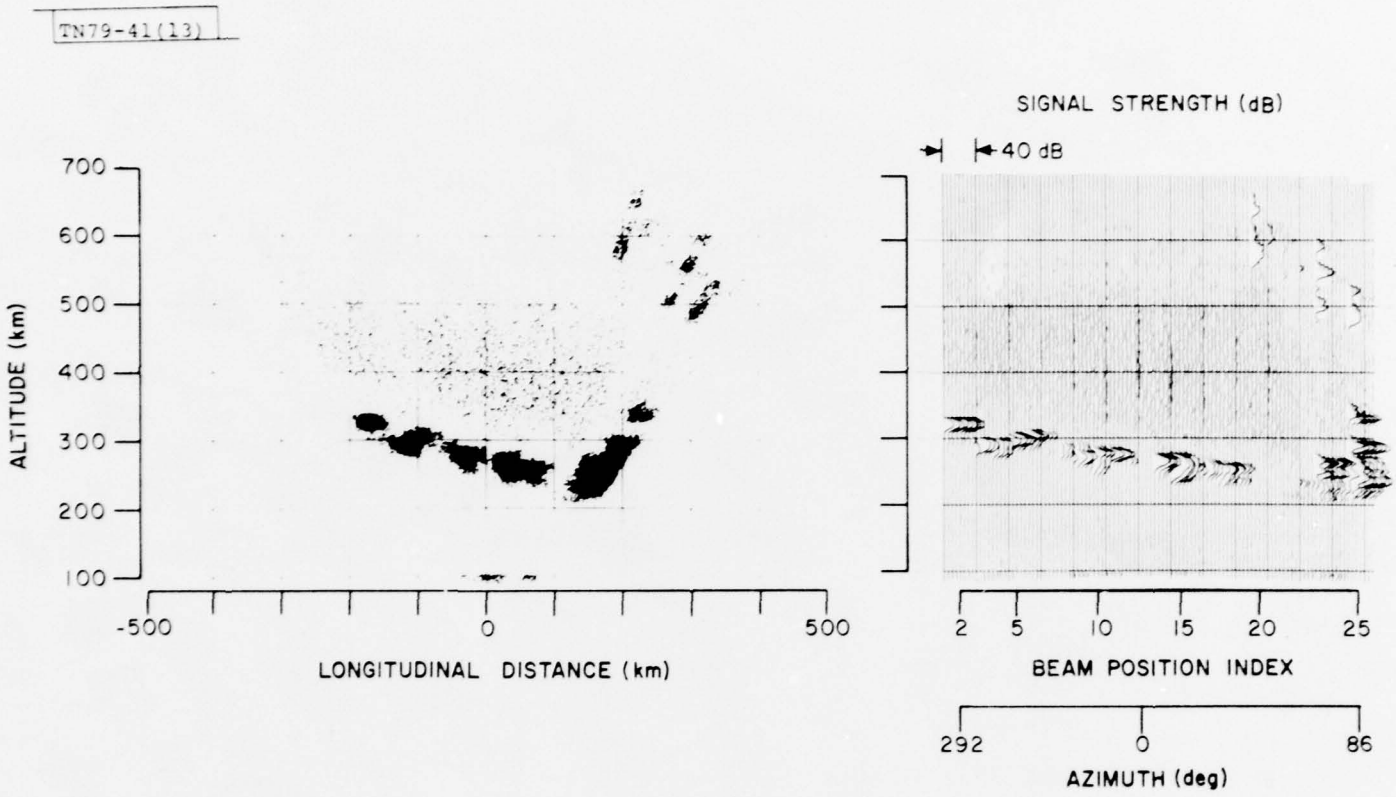

Fig. 13. UHF echo map and signal strength plot for 08:58:01 GMT scan.

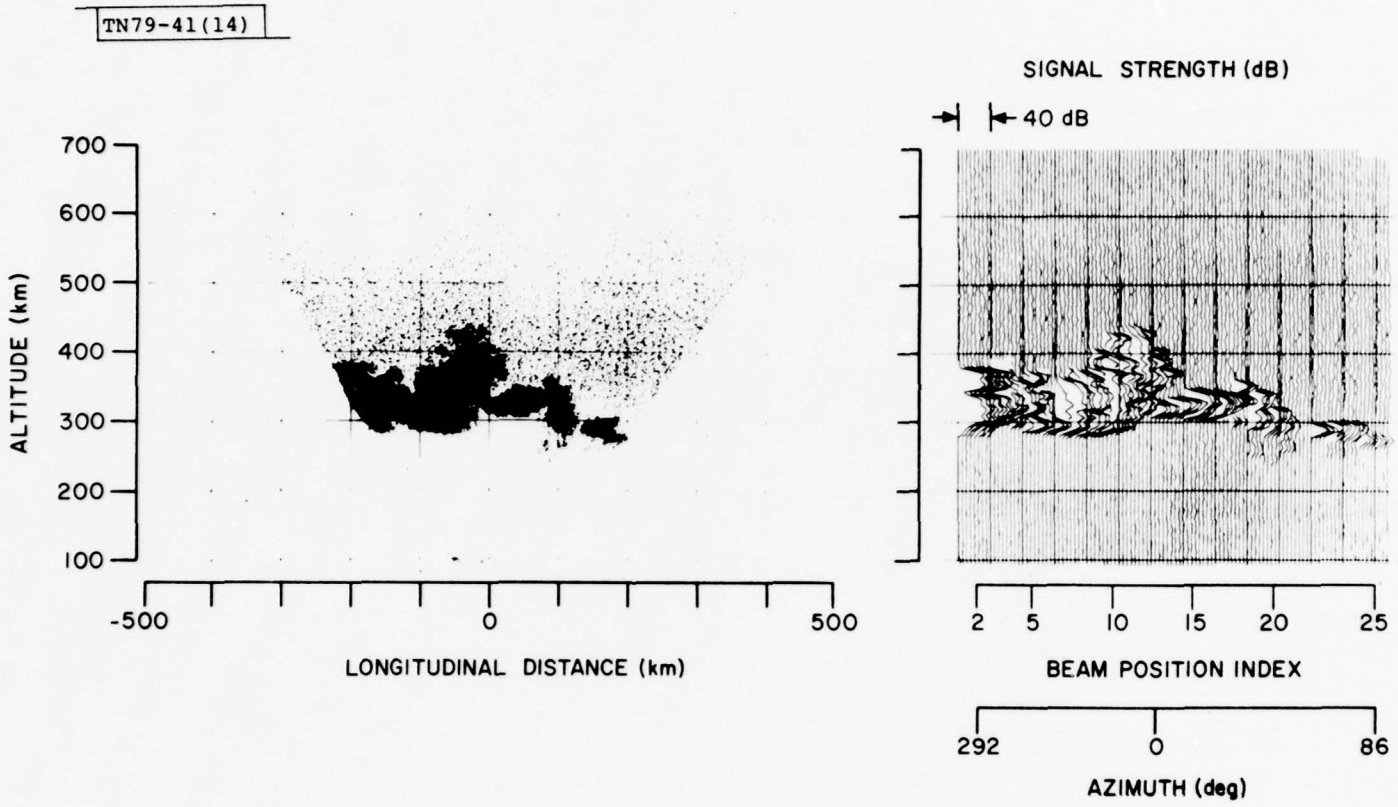

Fig. 14. UHF echo map and signal strength plot for 09:39:32 GMT scan.

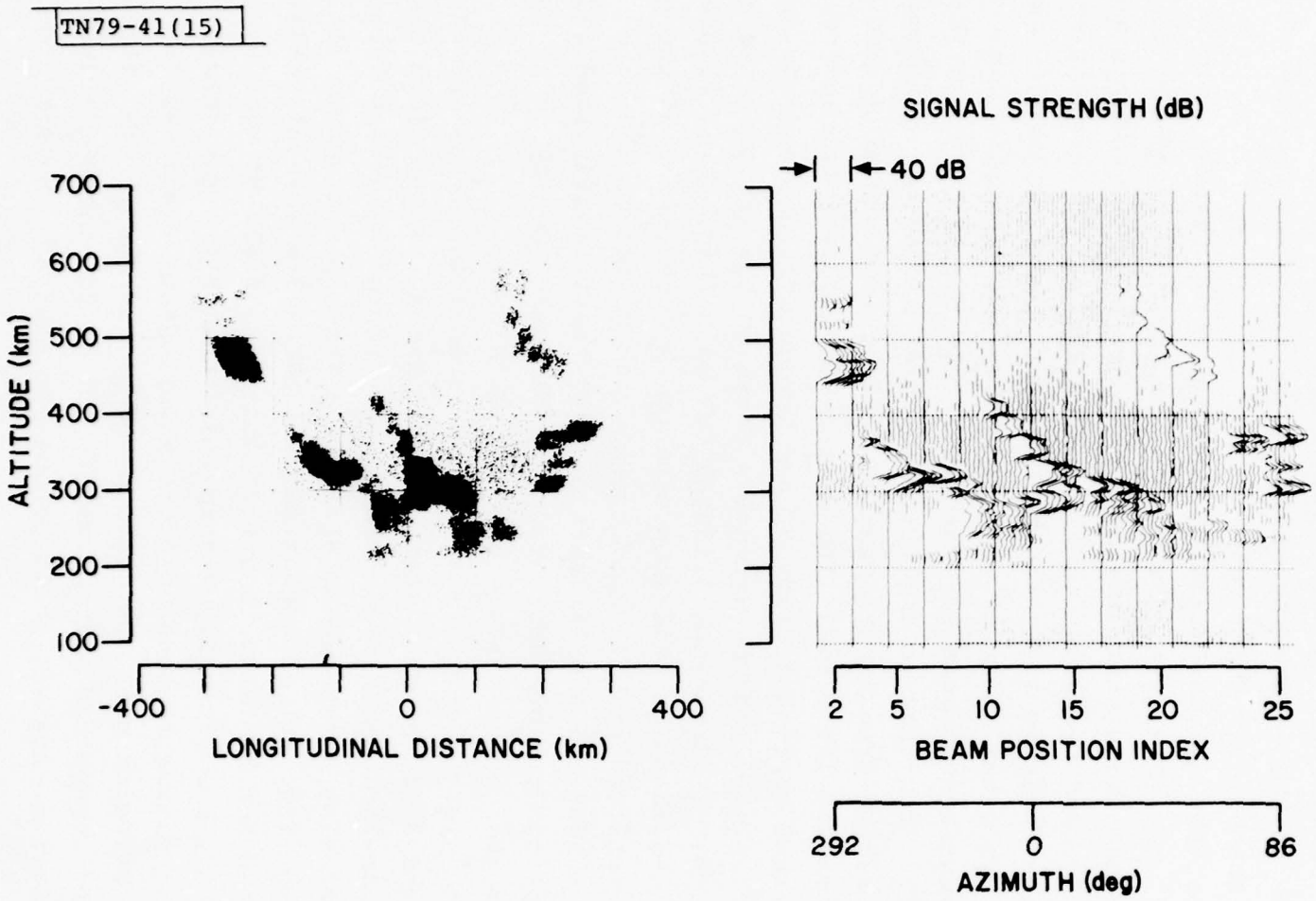

Fig. 15. UHF echo map and signal strength plot for 11:31:31 GMT scan.

of the antenna beam to the geomagnetic field lines above 400 km altitude in the northeast, allowed only transient records of the signal strength in that region.

The echo map and signal strength plot of the UHF scan at 11:41:47 GMT (Fig. 16) show not only a rapid decay of the scattering irregularity regions, but also a marked reduction in the background F-region density in the altitude interval just below the decaying irregularity regions. These depleted plasma regions were not observed earlier during the expansive phase of the irregularity regions. The plots from the 11:56:52 GMT scan (Fig. 17) show that as the irregularities dispersed, the depleted plasma region grew. Both regions drifted eastward at a rate of approximately 120 m/sec. The continued dispersal of the irregularity region, the continued drift of the irregularities, and the growth of the depleted plasma region are shown in the plots of the UHF data acquired during the 12:04:05 GMT scan (Fig. 18). Figure 18 shows also that the peak echo strength at the center of the echo region remained strong while the top and bottom of the echo region eroded. The drift rate of both the irregularities and the depleted regions decreased significantly shortly after this but remained approximately equal to each other.

The plots from the 12:18:06 GMT scan (Fig. 19) show continued drift and decay of most of the echo regions. These plots also show a newly formed local irregularity region below the F-region bottomside at about 240 km altitude. The plots from the 12:24:28 GMT scan (Fig. 20) show that most of the 3/8 m irregularities, which had not had time to drift out of the field-of-view by 12:30 GMT, had virtually dissipated. One of the remaining depleted plasma regions is still prominent in the lower to middle F-region near the western end of the scan. The other depleted region had drifted nearly out of the field-of-view, but its trailing edge was still detectable near the eastern edge of

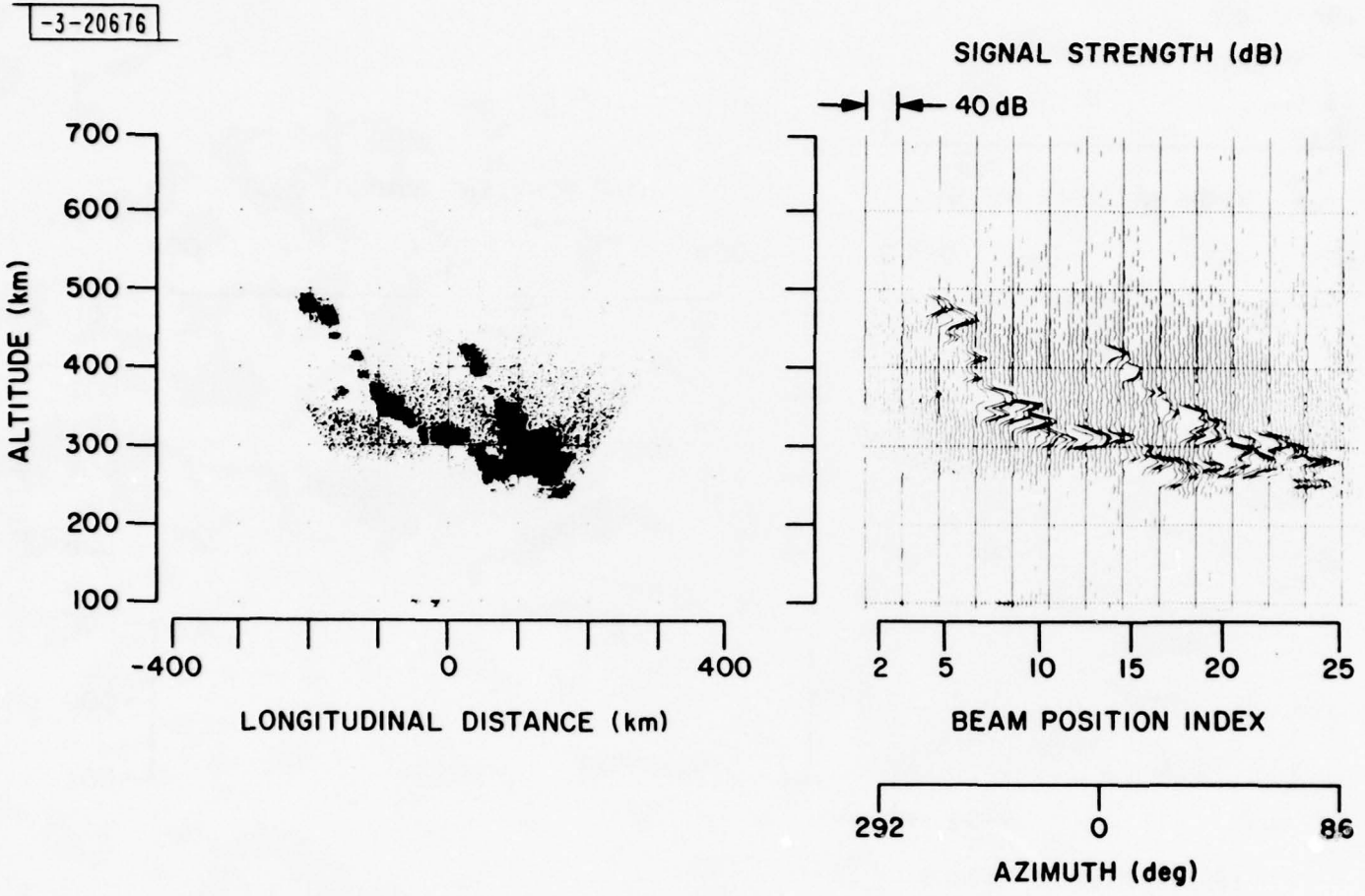

Fig. 16. UHF echo map and signal strength plot for 11:41:47 GMT scan.

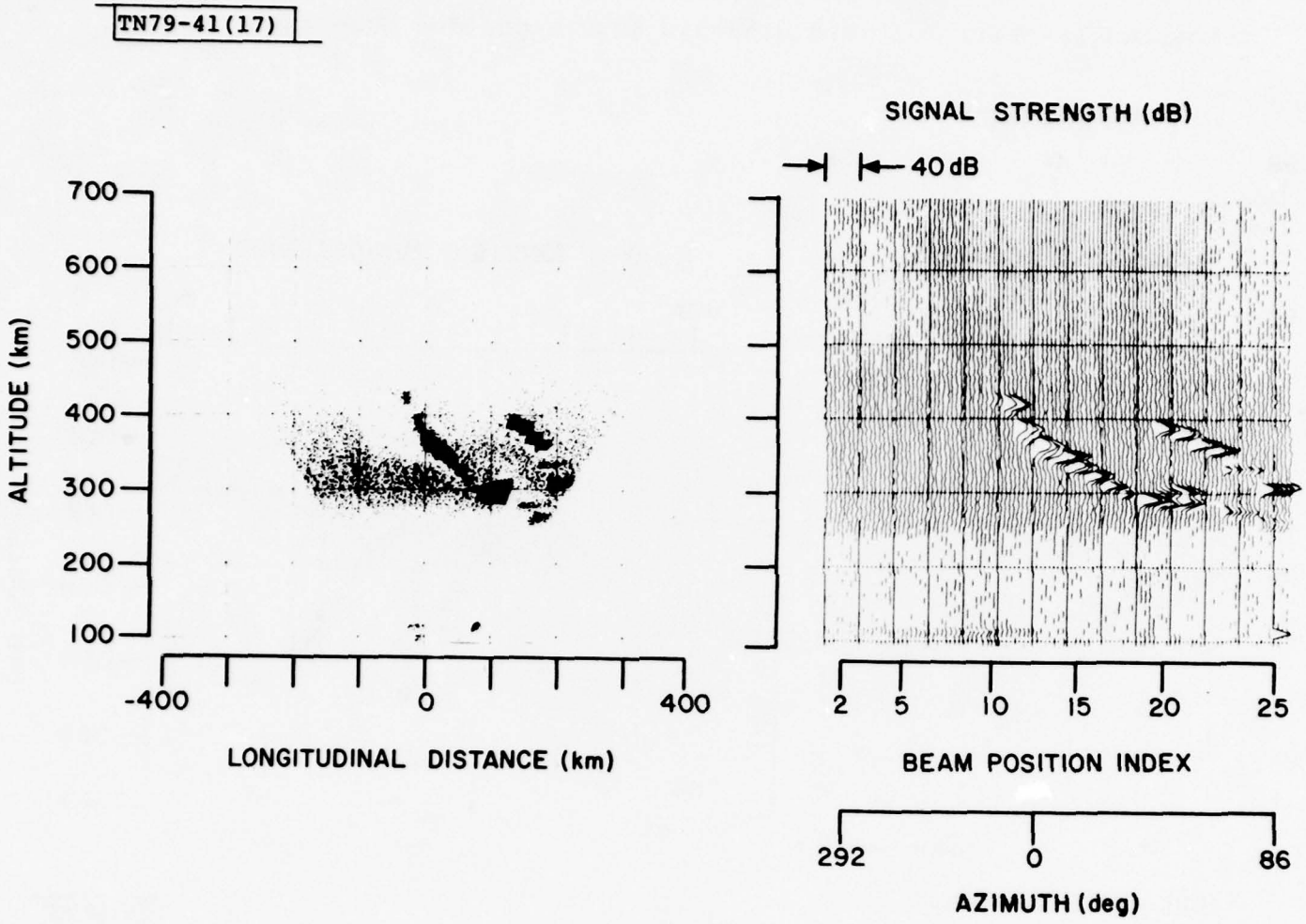

Fig. 17. UHF echo map and signal strength plot for 11:56:52 GMT scan.

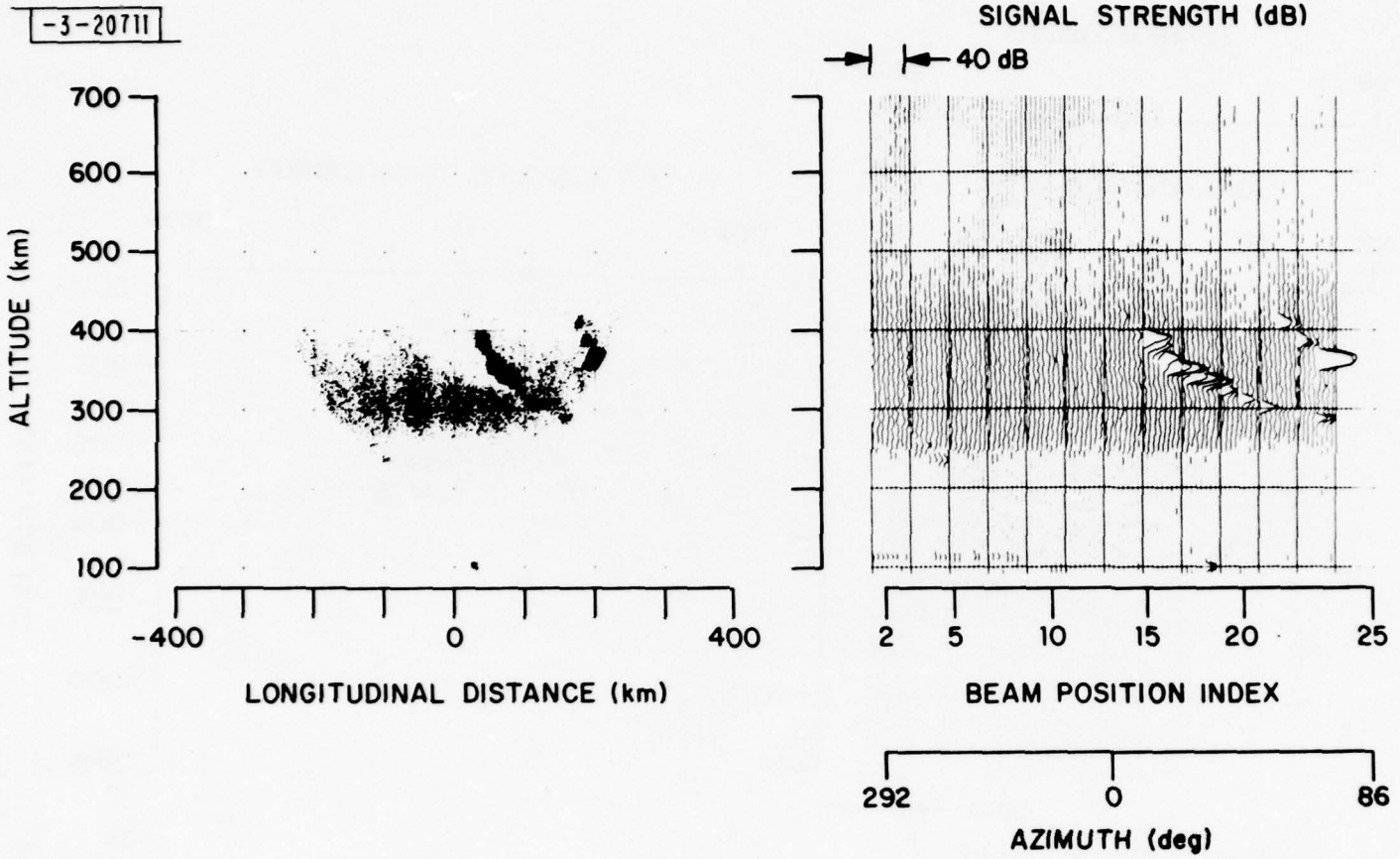

Fig. 18. UHF echo map and signal strength plot for 12:04:05 GMT scan.

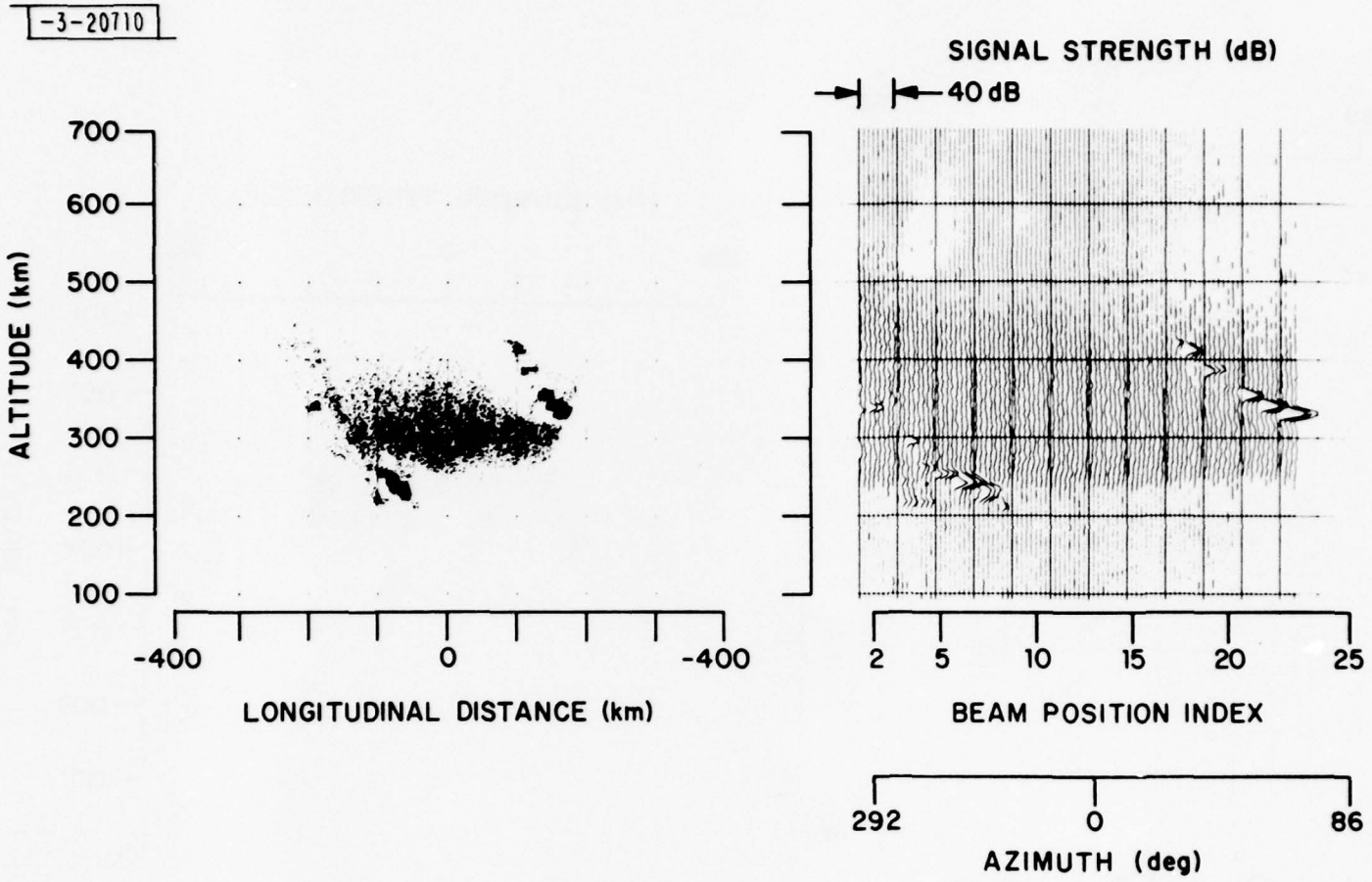

Fig. 19. UHF echo map and signal strength plot for 12:18:06 GMT scan.

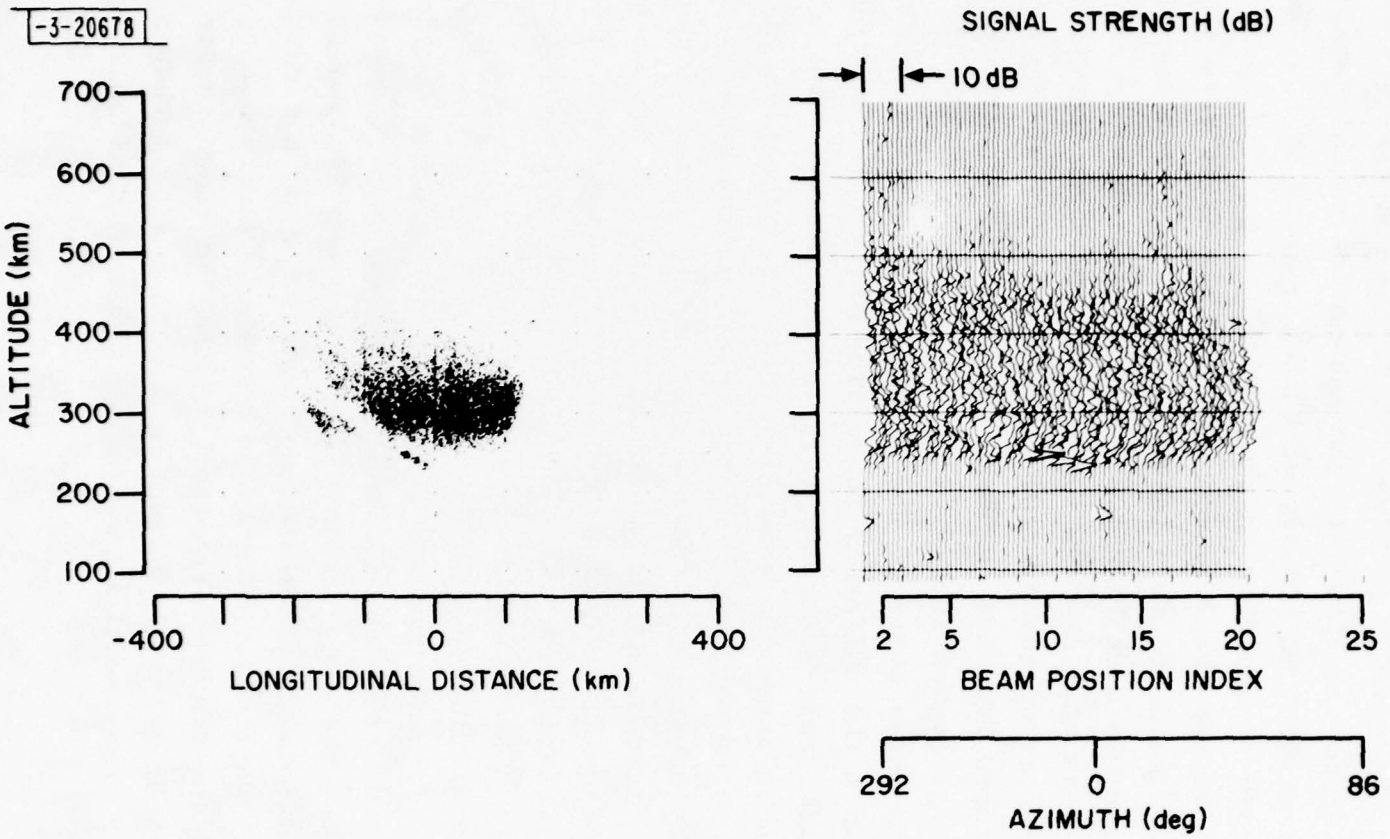

Fig. 20. UHF echo map and signal strength plot for 12:24:28 GMT scan.

the scan on the topside at 12:30 GMT as the observations for that night were ended. A trough in the incoherent signal background is graphically evident in the signal strength plots of Fig. 20 despite the stochastic fluctuation in the signals.

A plot of the easterly component of the drift rate is shown in Fig. 21. The drift rate increased uniformly from the start of the measurements at F-region sunset, until about 12:15 GMT (i.e., until about 1 AM true local time) and then decreased rapidly. A plot of the average altitude history of the bottomside as deduced from the UHF echo maps and the electron density profiles is presented in Fig. 22.

The expansive phase of the irregularity regions as observed coincided with the uniformly increasing drift rate, starting when the drift rate was relatively low (90 m/sec). The decay phase began at about the same time that the inflection in the drift rate curve occurred. Ad-hoc relationships between the irregularity development and the rise and fall rate of the bottomside altitude are not obvious. However, it may be noted that the bottomside had risen above 300 km altitude at the start of the irregularity formation and had fallen below 250 km at the time of their disappearance.

C. Scintillation Data

A satellite (Object No. 3605) passed above the irregularity region in the northeast at 10:18 GMT and was skin tracked by ALTAIR. At that time, the echo region extended between 270 and 430 km altitude uniformly distributed horizontally from the northwest through the northeast. The radar signal intensity during a short section of the track (calibrated in dBsm) is shown in Fig. 23. The satellite, a stabilized cylinder with a slowly varying normal backscatter cross section, was at an altitude of 1450 km. As

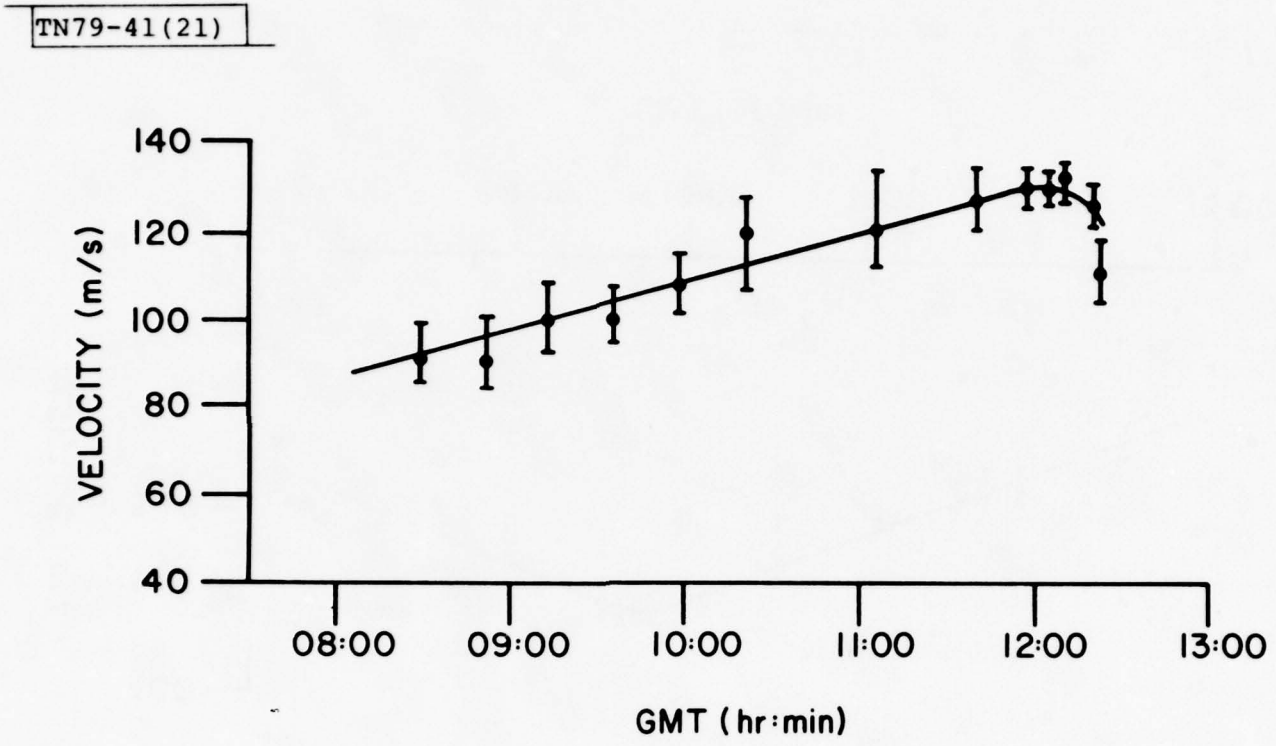

Fig. 21. Easterly drift rate of echoes on 11 August, 1978.

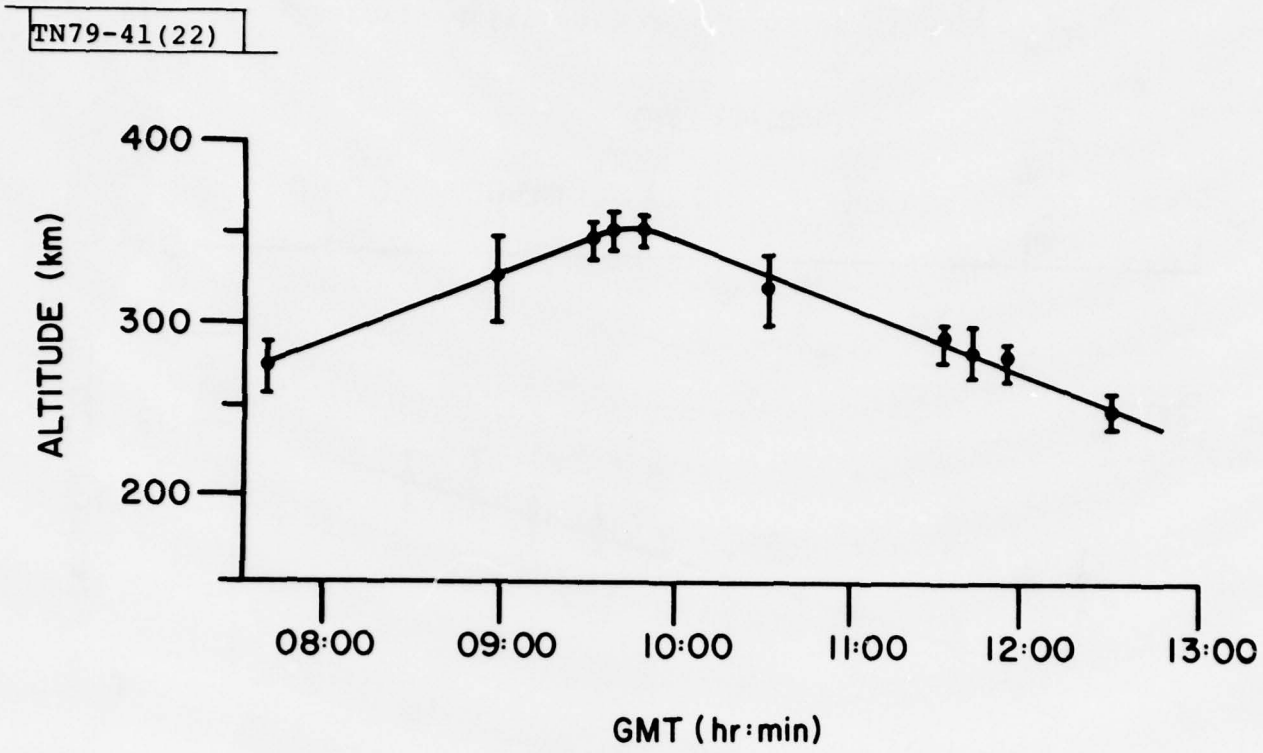

Fig. 22. Altitude history of F-region bottomside on 11 August, 1978.

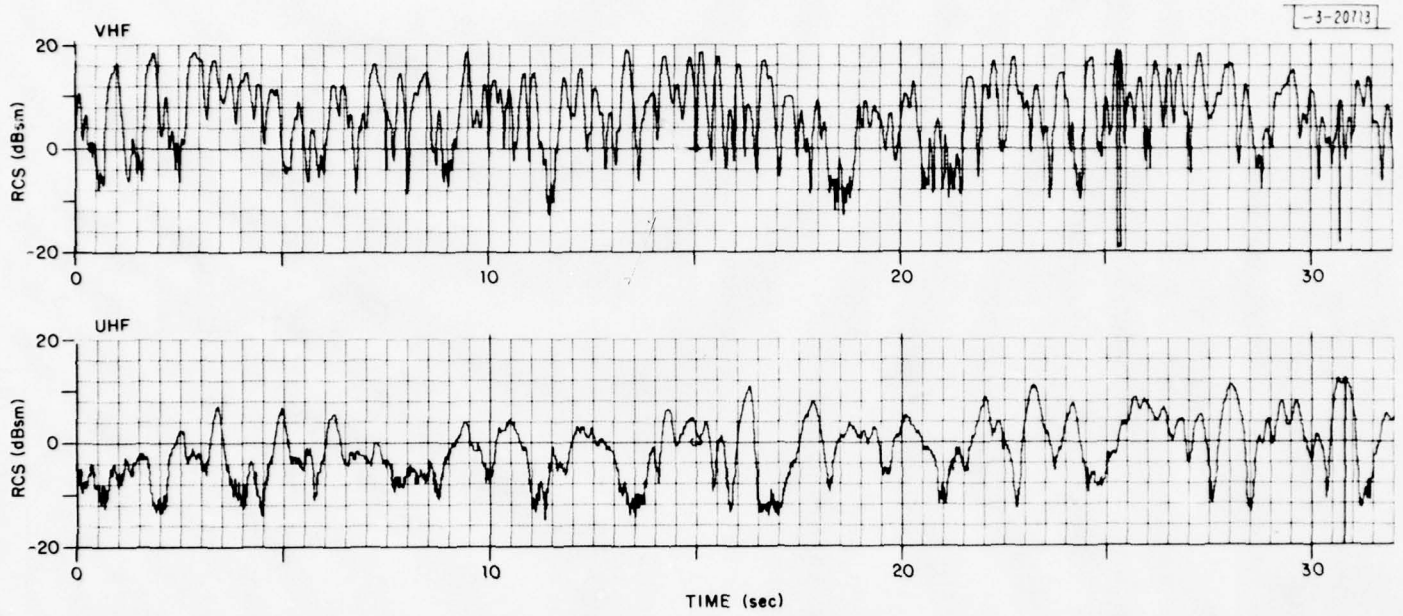

Fig. 23. Scintillation signals satellite no. 3605, T_o = 10:18 GMT, 11 August, 1978.

indicated in Fig. 23, saturating scintillation occurred at both VHF and UHF when the satellite passed above the ionospheric region where strong quasi-coherent echoes were observed. The faster fading rate of the VHF signal relative to the UHF signal seen in Fig. 23 is characteristic of strong ionospheric scintillation. For comparison, the same satellite was tracked through the smooth daytime ionosphere and the corresponding cross sections are shown in Fig. 24. Detailed correlation of the scintillation signals with the backscatter echoes has not yet been attempted.

D. Ionospheric Density Profiles

Density profiles of the F-region were derived from the UHF backscatter signals. Since the radar receiver output signals were calibrated in terms of an equivalent point target cross section, the absolute value of the electron densities may be obtained directly from these measurements without need to employ secondary calibrations. The relationships are derived in Appendix A, where the assumption is made that the nighttime electron temperature is approximately equal to the nighttime ion temperature. Errors in the results due to this approximation are not expected to be significant.

Electron density profiles were calculated for each of the geomagnetically orthogonal scans as well as for some individual beam positions with the antenna elevation angle off-set several beamwidths below orthogonality. When irregularities were present, portions of the density profiles were often contaminated by the much stronger quasi-coherent echoes. However, due to the favorable range resolution and the wide dynamic range of the radar, these regions as a rule only affect a small portion of the profiles and are readily recognizable. Therefore, no attempt was made to edit these sections or to label them as false values of the derived densities. To some extent, their presence in the profile displays is useful to indicate relationships between the

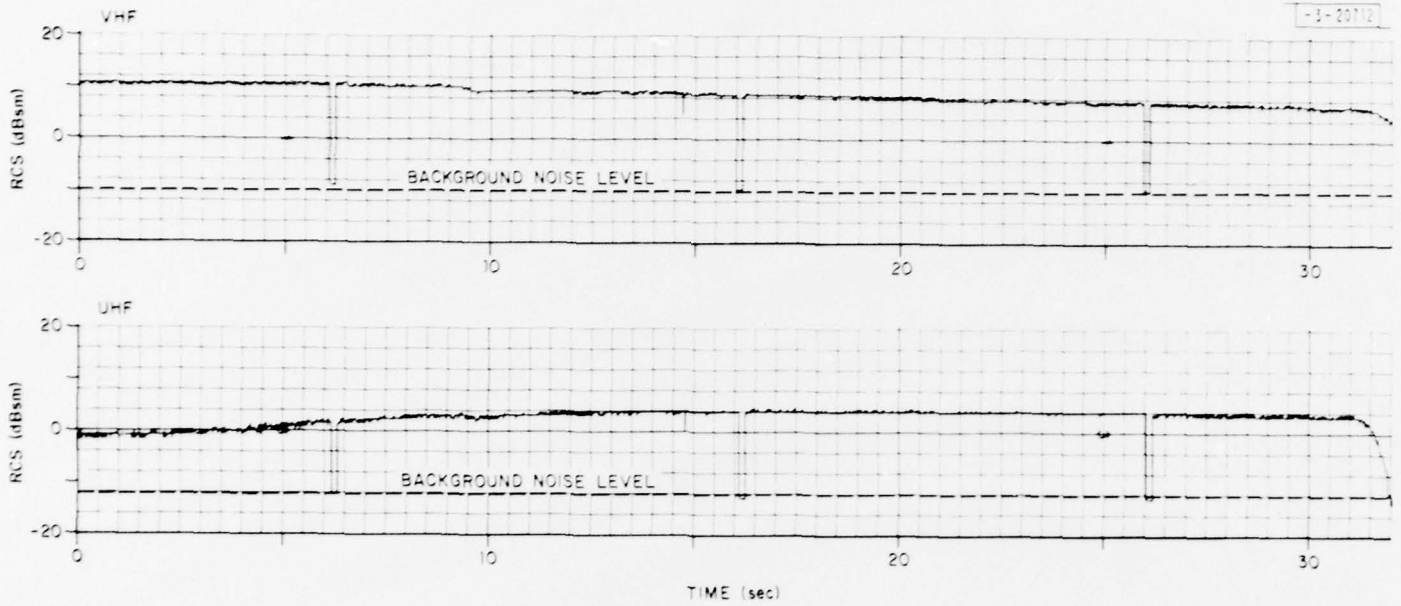

Fig. 24. Satellite radar cross section, satellite no. 3605, 14 August, 1978.

irregularities and larger scale density gradients. For the off-orthogonal beam signals, some contamination occasionally occurred when very strong quasi-coherent echoes entered through the antenna sidelobes. However, this problem of sidelobe clutter is much less severe at UHF than at VHF.

An integration time of 9 sec was used in processing the density profiles derived from signals recorded during antenna scans consistent with the antenna dwell times. One consistent exception was for the central beam position signals where the dwell time was short and the integration time was limited to 1 sec. Consequently, the profile for this position, indicated on the plots as beam position 13, is more ragged than the others. During processing, a threshold was set on the minimum signal processed at 0.2 dB above RMS system noise. This resulted in a smooth profile limit in regions where the density was too low to measure. For signals derived from non-orthogonal beam positions, integration times between 8 and 40 sec were used.

Figure 25 shows the electron density profiles for each beam position for the partial scan starting at 07:40:18 GMT, prior to meter sized irregularity formation. The F-region thickness at that time was, as expected, appreciably greater than later in the evening. The peak electron density was relatively high, nearly $10^{12}/m^3$. The bottomside was at an altitude of 275 km at 150 km west of the radar and at 300 km altitude at 75 km east of the radar.

The electron density profiles for the antenna scan at 08:58 GMT are shown in Fig. 26. At this time, the quasi-coherent backscatter from the irregularities, which had recently formed in the steepest gradient region of the bottomside, contaminate the density measurements in that region, but do not bother appreciably the remainder of the profiles. Also, at that time, there were strong quasi-coherent echoes in the topside

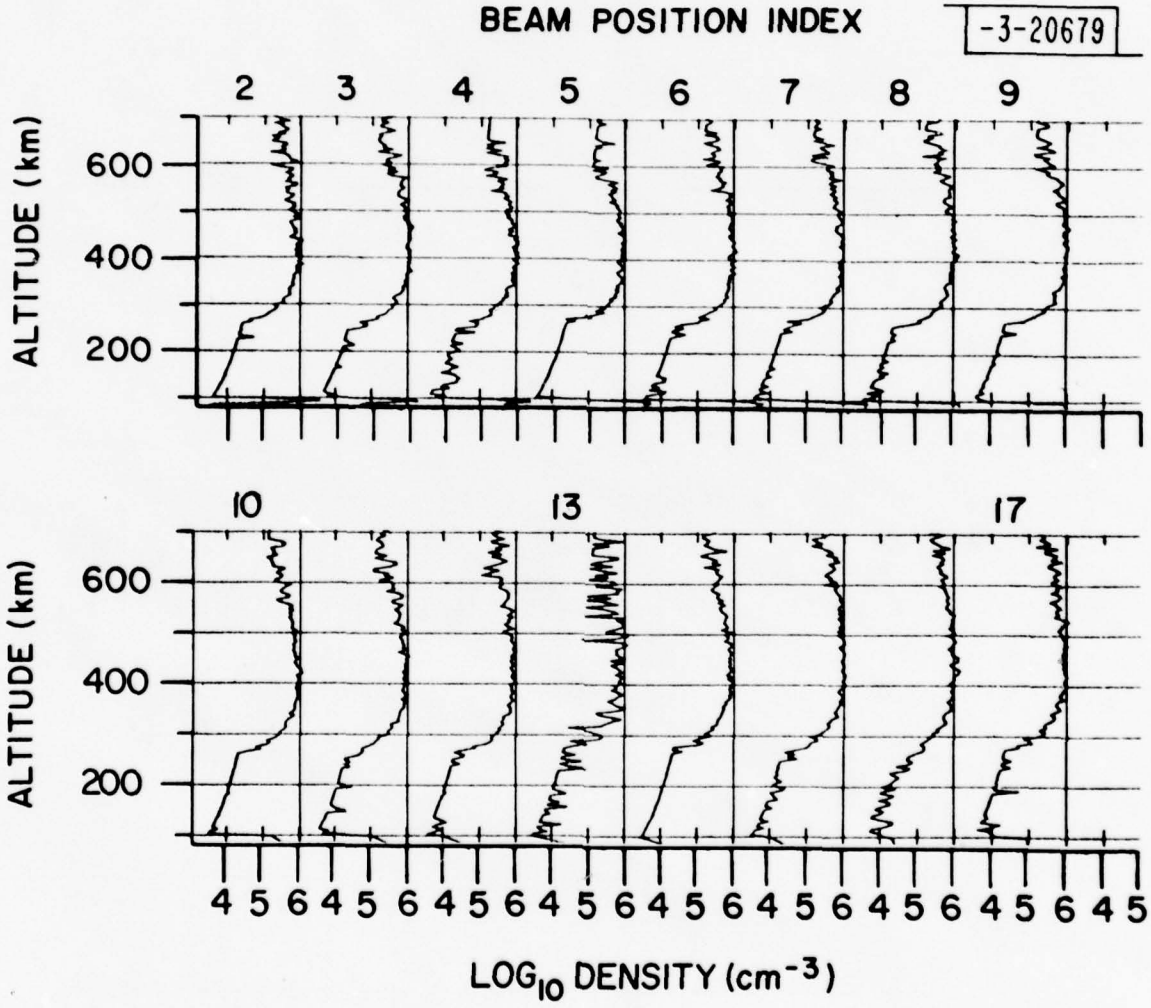

Fig. 25. Electron density profiles for beam positions 2 through 10 during 07:40:18 GMT scan.

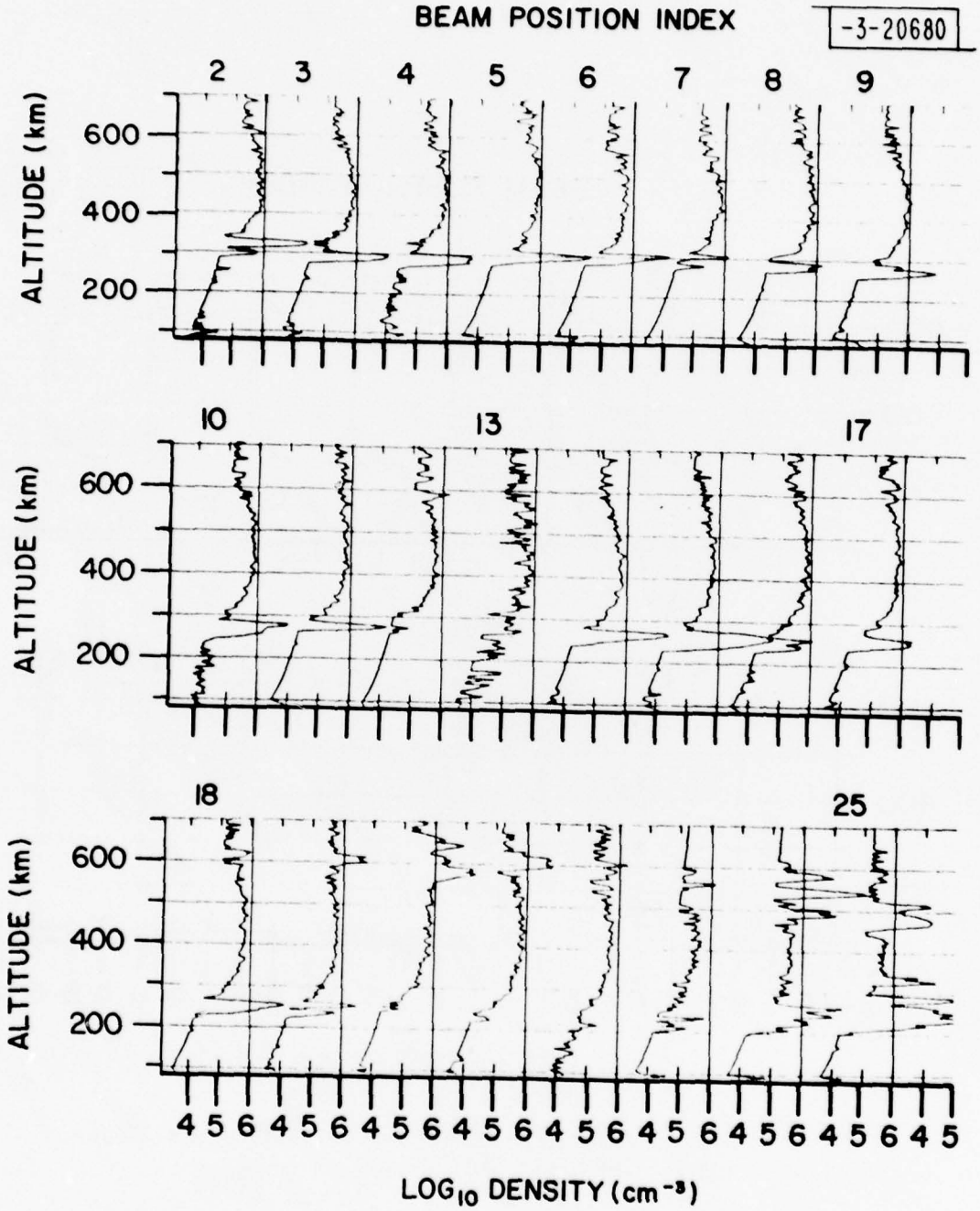

Fig. 26. Electron density profiles for sequential beam positions during 08:58 GMT scan.

steepest gradient region in a few of the most eastern beam positions. The density profiles from this scan and the earlier scan show no indication of the occurrence of biteouts (plasma depleted regions) in the middle of the F-region, even though irregularities are prominent on the topside at these times.

Density profiles for off-orthogonal (to geomagnetic field lines) beams are shown in Figs. 27 and 28. The profile in Fig. 27 was taken at 09:33 GMT with the antenna pointed toward magnetic north and with the elevation angle set 7^{o} below the orthogonal position. Figure 28 shows the electron density profile at 09:37 GMT, where the antenna is pointed northwest and the elevation angle is set 5^{o} below orthogonality. The F-region layer was then thinner in the northwest, with a smaller electron content than in the north. No plasma depleted regions were detected during these observations.

Density profiles for each beam position of the orthogonal scan starting at 09:40 GMT are shown in Fig. 29. On the western side of the scan, bottomside irregularities have expanded up into the middle of the F-region, obscuring the density measurements over a wide region in that sector. It is of interest to note that the strength of the quasi-coherent signals were about the same in the bottomside layer, where the density is an order of magnitude smaller than the peak, as in the peak density region.

Density profiles for each beam position during the orthogonal scan starting at 11:31 GMT are shown in Fig. 30. Quasi-coherent echoes which were then scattered through the region obscure parts of the profiles. Troughs in the density profiles near the middle of the F-layer, just below the irregularity echoes, particularly for the first beam position on the west end, between 350 and 450 km altitude and in the next to last beam position toward the east at an altitude of 350 km were then evident. These troughs are believed to be true manifestations of depleted

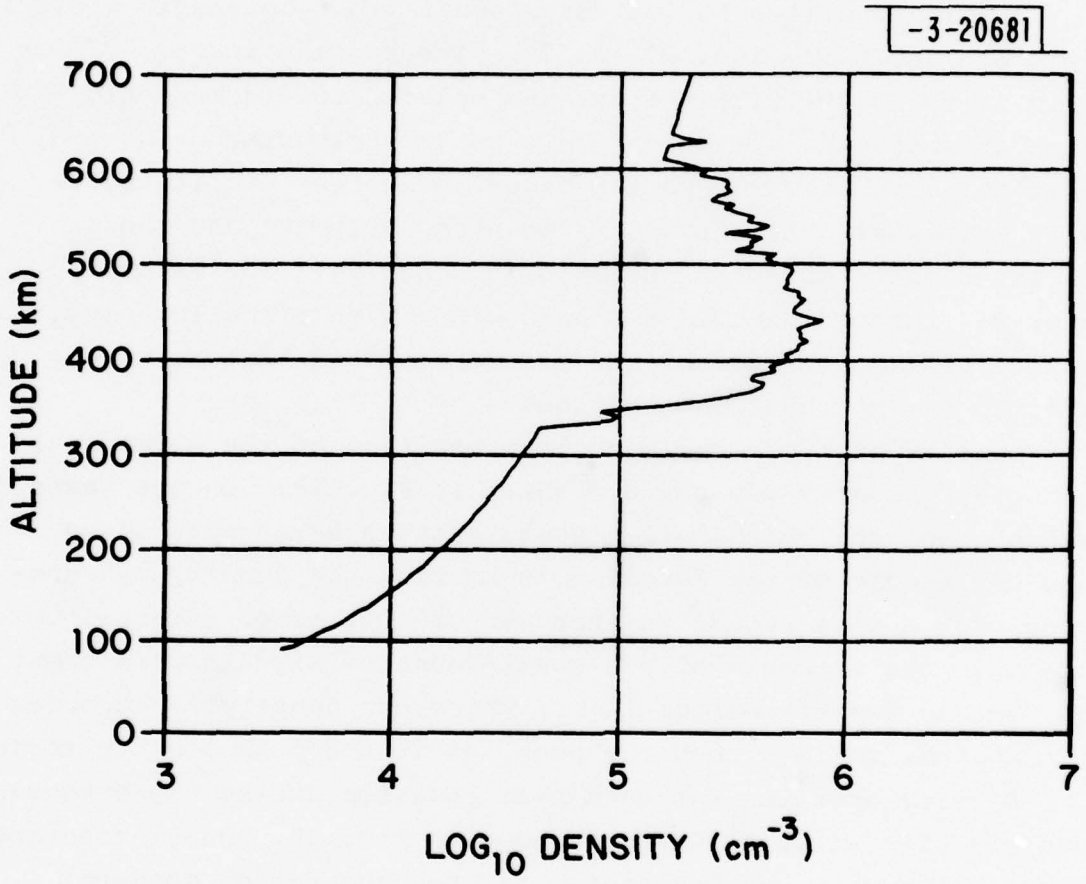

Fig. 27. Electron density profile for beam position at azimuth = 8.4°, elevation = 74° during 09:33 GMT scan.

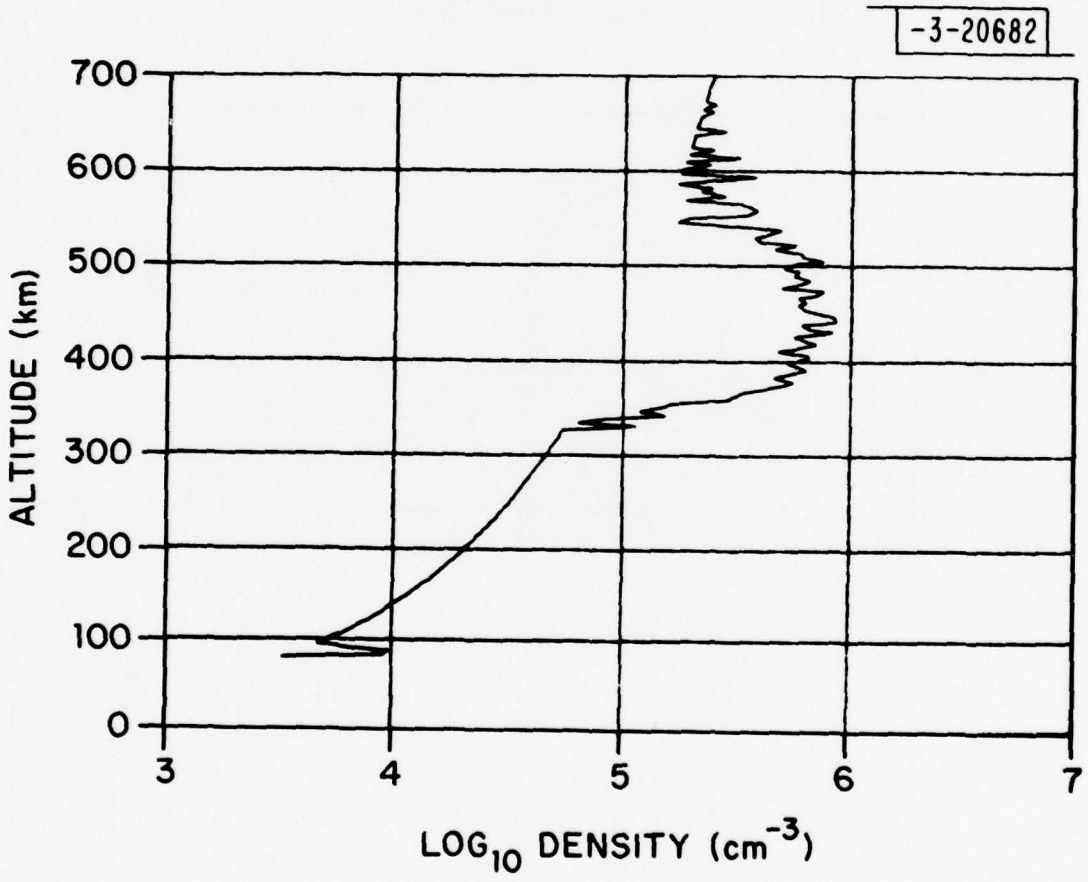

Fig. 28. Electron density profile for beam position at azimuth = 300°, elevation = 60° during 09:37 GMT scan.

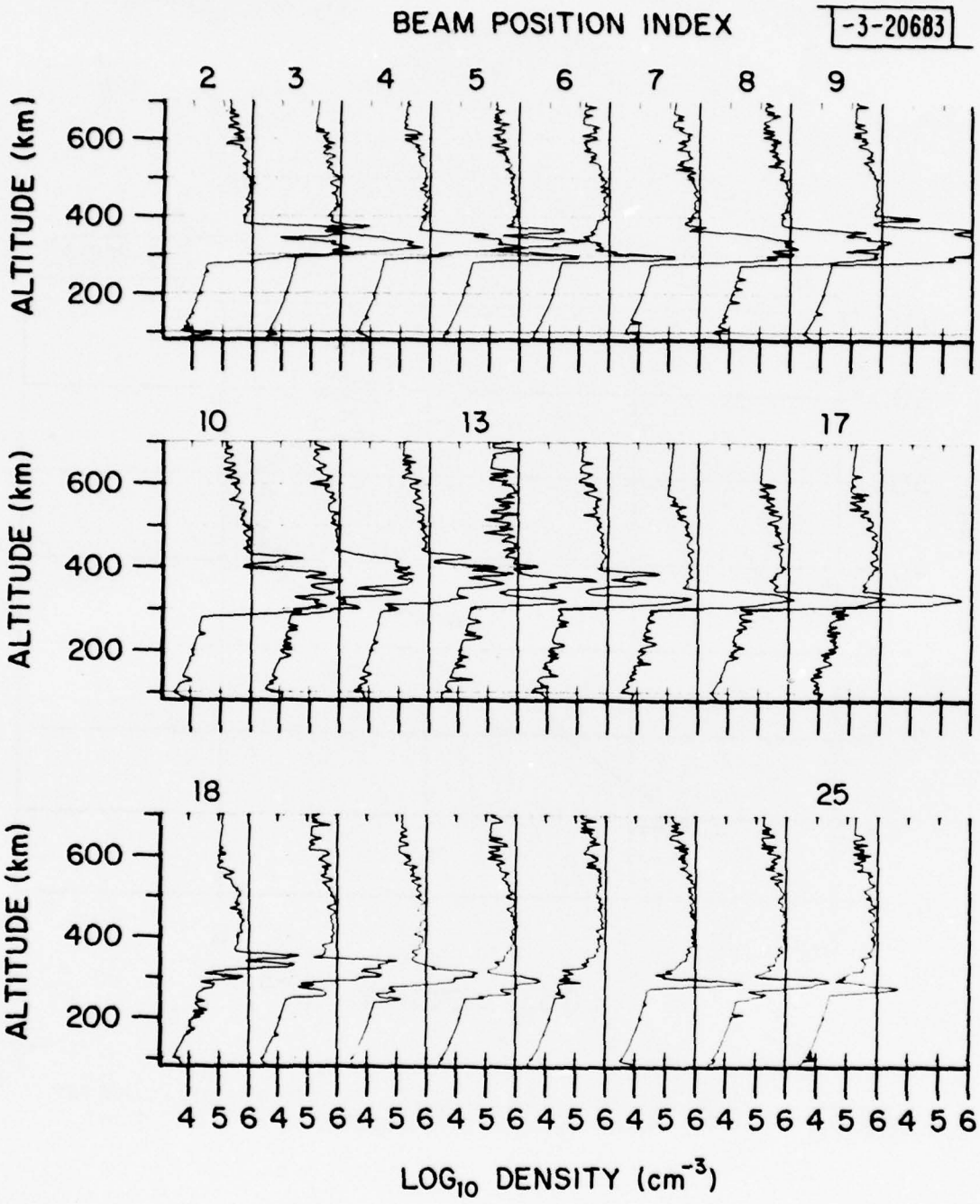

Fig. 29. Electron density profiles for sequential beam positions during 09:40 GMT scan.

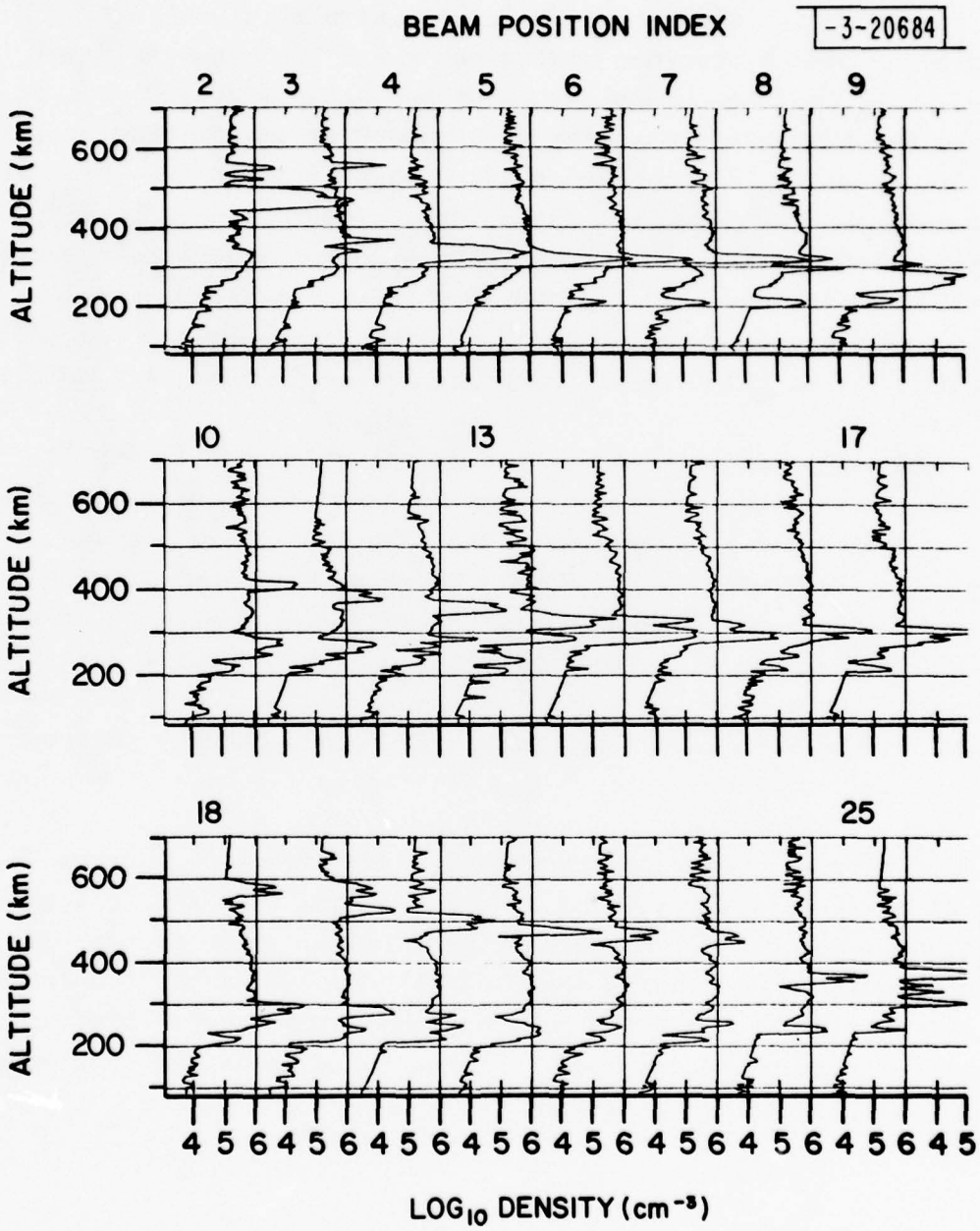

Fig. 30. Electron density profiles for sequential beam positions during 11:31 GMT scan.

plasma regions. Support for this assertion is given in Figs. 31 and 32, profiles recorded toward the north for non-orthogonal beam positions. An unmistakable biteout of almost an order of magnitude below the peak density appeared at an altitude of 375 km at 11:38 GMT. Successive measurements at 11:38 GMT (Fig. 31) and at 11:39 GMT (Fig. 32) showed the biteout to be widening, rising, and filling in. The biteout appeared in the beam positions further to the east at 11:42 GMT with its leading edge at a lower altitude as shown in Fig. 33. The later observation indicates that the biteout layer was tilted downward and drifting to the east.

Density profiles for the orthogonal scan at 11:49 GMT (Fig. 34) show the first four beamwidths in the west had become clear of 3/8 m irregularities. The next four beams contain topside irregularities and middle F-region biteouts. Profiles for the orthogonal scan at 12:18 GMT (Fig. 35) show most of the beams to be clear of irregularity echoes, except for a narrow layer on the bottomside in the northwest and in the middle F-layer to the east. Depleted plasma regions occurring just below the remaining middle F-layer irregularities in the east were evident at that time.

The density profiles for the last orthogonal scan from 12:24 to 12:30 GMT presented in Fig. 36 show that the irregularity regions previously seen had mostly vanished. Some of the irregularities previously seen had drifted out of the truncated field-of-view to the east and others had dissipated. Plasma depleted regions in the middle of the F-region in the west were still visible as shown in Fig. 36.

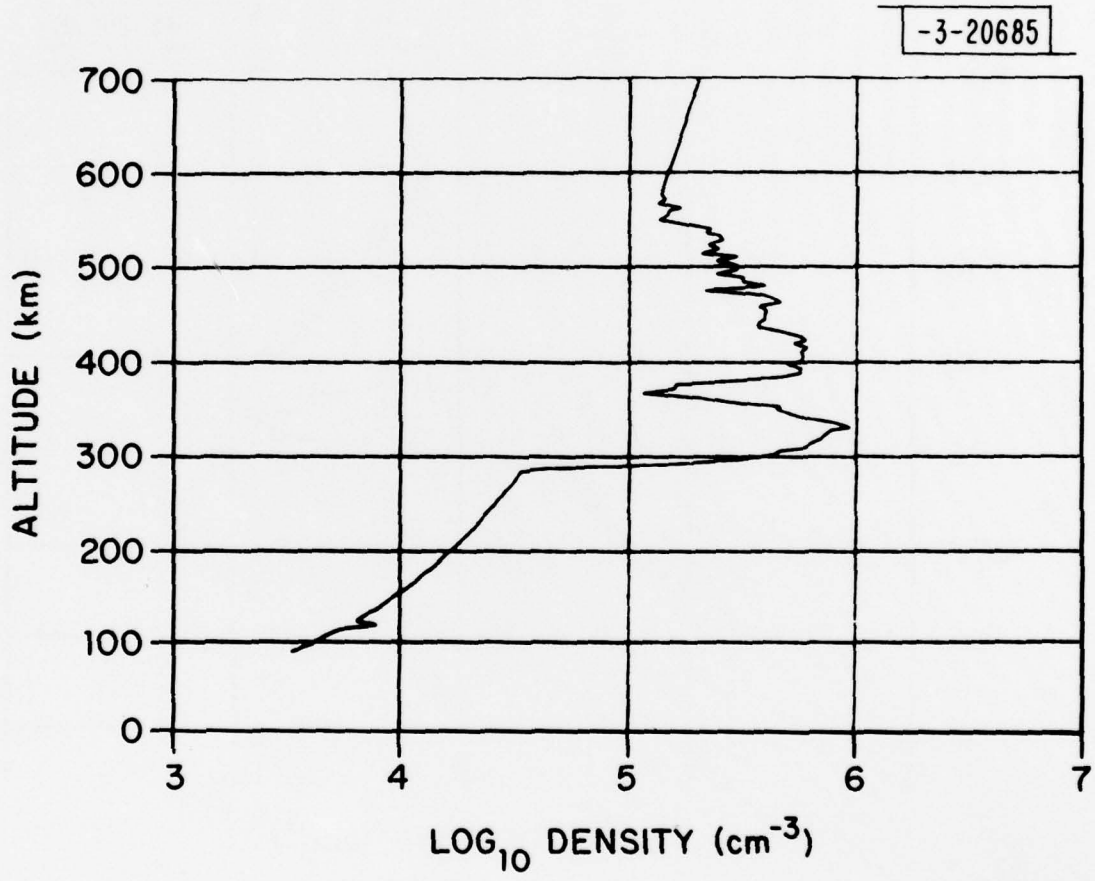

Fig. 31. Electron density profile for beam position at azimuth = 8.4°, elevation = 74° during 11:38 GMT scan.

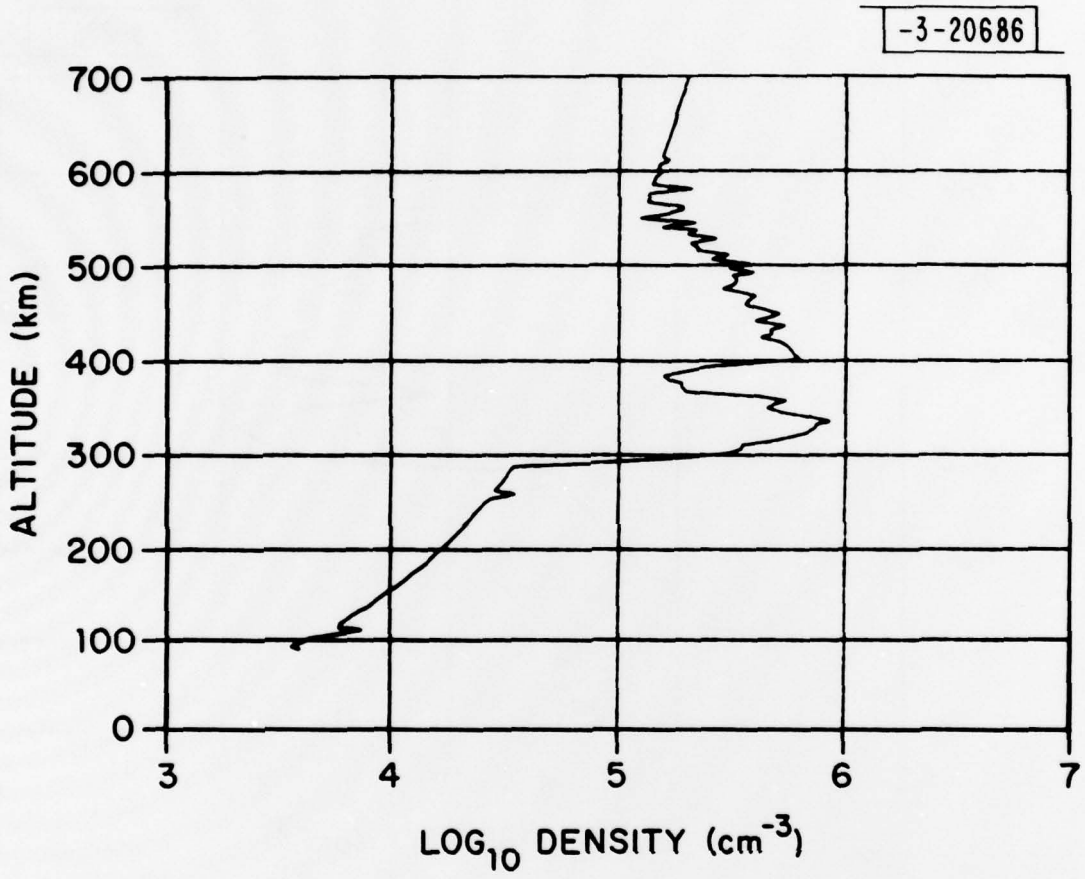

Fig. 32. Electron density profile for beam position at azimuth = 8.4°, elevation = 74° during 11:39 GMT scan.

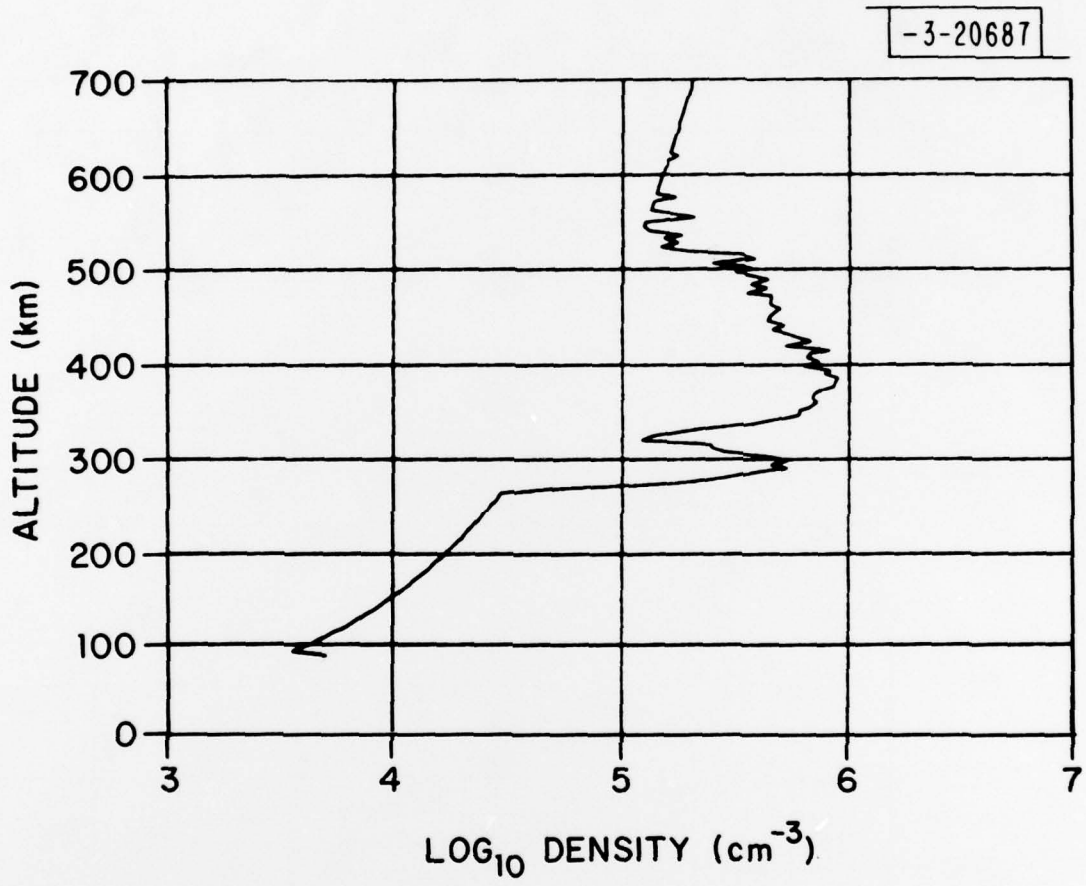

Fig. 33. Electron density profile for beam position at azimuth = 34°, elevation = 75° during 11:42 GMT scan.

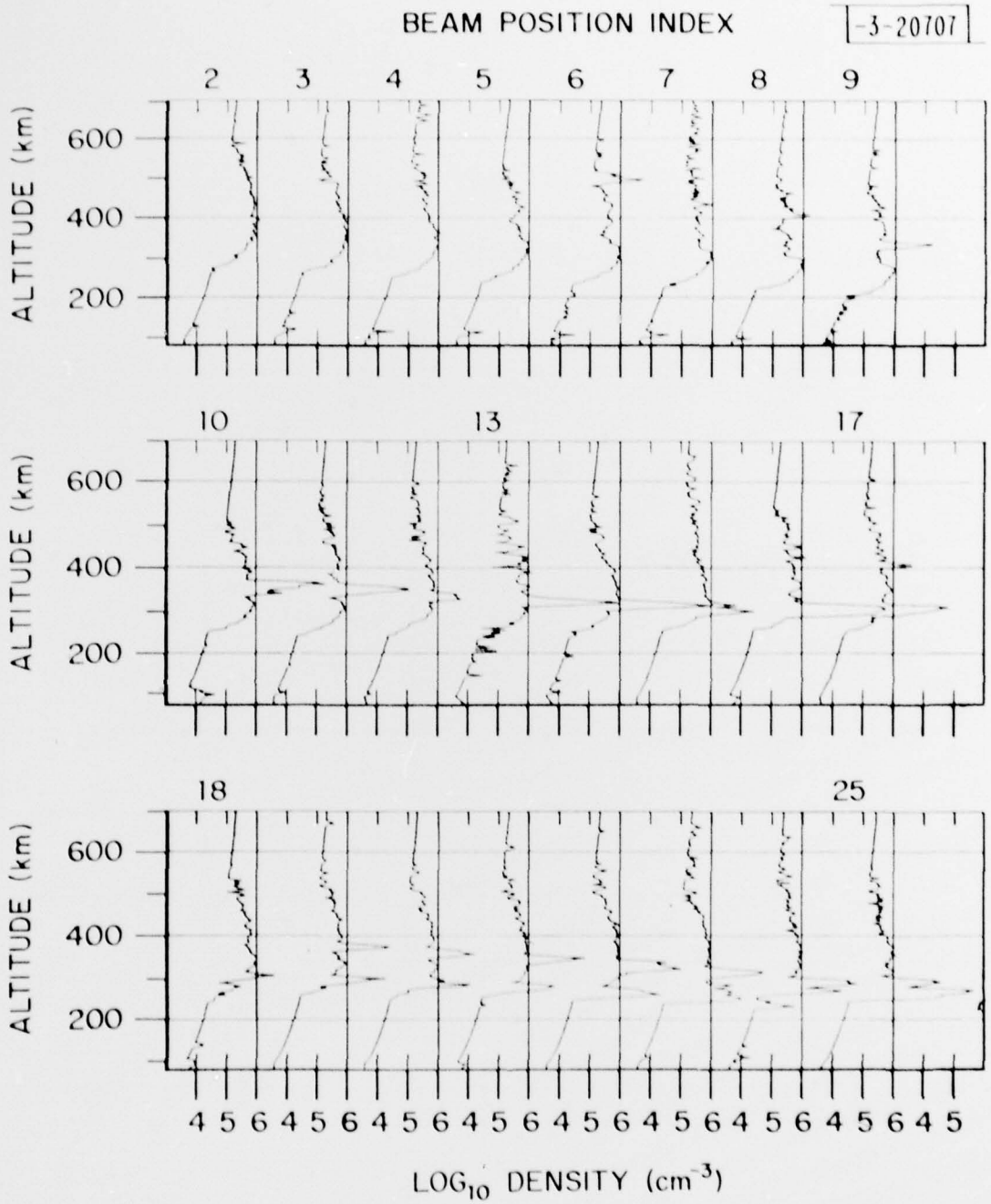

Fig. 34. Electron density profile for sequential beam positions during 11:49 GMT scan.

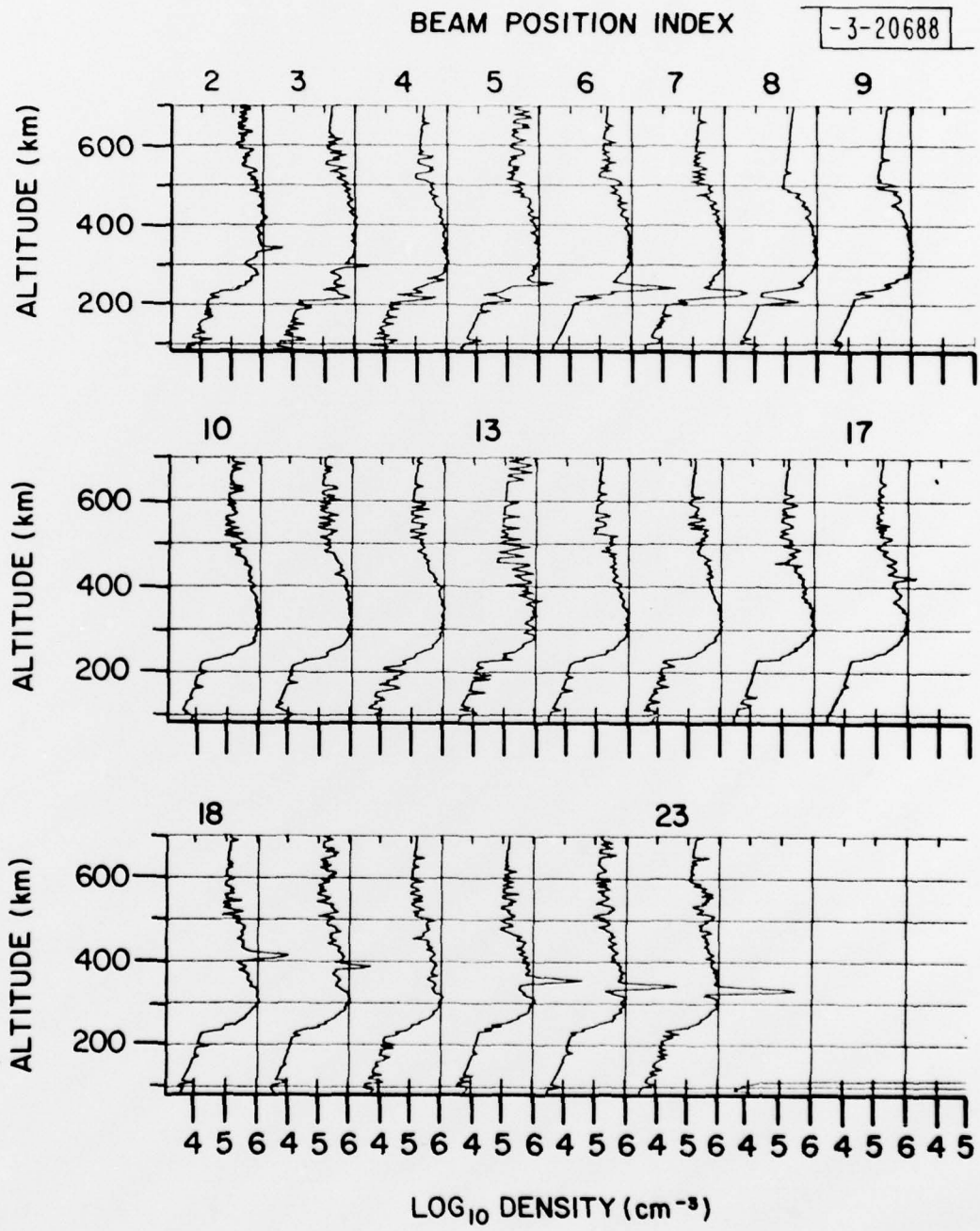

Fig. 35. Electron density profiles for sequential beam positions during 12:18 GMT scan.

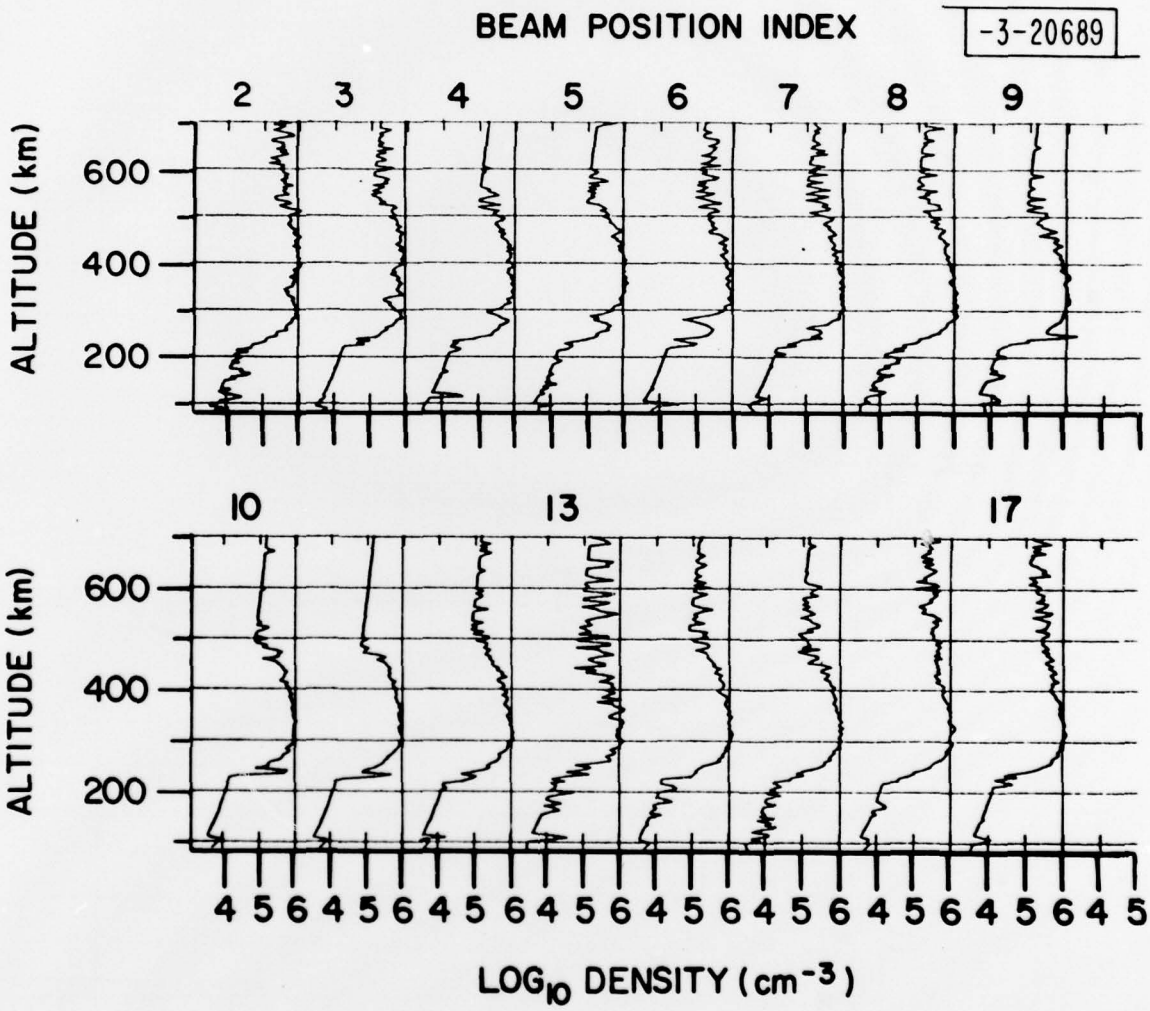

Fig. 36. Electron density profiles for sequential beam positions during 12:24 GMT scan.

IV. DISCUSSIONS AND CONCLUSIONS

The experimental results described in the previous sections have numerous significant implications for theoretical modeling and prediction of ionospheric irregularities. A few of the most obvious ones are discussed here.

A. Spectral Slope in the Submeter Scale Size Region

Ionospheric irregularities in the tens of kilometers to tens of meters scale size region are generally agreed to obey a power law distribution. Recent speculation (Woodman, R. and S. Basu, October 1978) suggests that the inner scale size of this distribution occurs at the ion gyro-radius, i.e., at a few meters, and that a different distribution law applies to the smaller sized irregularities. The existence of backscatter data at two wavelengths in this latter domain offers the opportunity to determine the spectral slope in this region.

The quasi-coherent radar echo signal is composed of the total contributions of the echoes from each of the many individual half-wavelength sized irregularities illuminated by the radar. Thus, the output signal level is a measure of the spectral-power at that wavelength and is proportional to the number of irregularities in the corresponding radar range cell. For consistency in regard to the echo region volume, cases in which the radar beam appears to be "filled" by the irregularity region need to be selected for this type of data analysis. Some assurance that this condition is met can be obtained by selecting data for which the echo regions are homogenous and appear to subtend larger angles at the radar than the antenna beam does. Under these conditions, the magnitude of the quasi-coherent signal tends to approach its historical maximum at a given range. To normalize the signal level independent of beam size, it is convenient to determine the signal level relative to the incoherent scatter

signal level which was measured at UHF and calculated at VHF for these data. As noted previously, the VHF quasi-coherent signal levels under these conditions were observed to be 45 to 47 dB above the calculated incoherent scatter signal levels and the UHF quasi-coherent signals were 34 to 37 dB above the measured incoherent echo levels.

A relationship for the ratio of quasi-coherent (P_{hF}) to incoherent (P_{hI}) signal levels as derived by Woodman, R. and S. Basu, October 1978 is

$$P_{hF}/P_{hI} = (\overline{\Delta N})^2 \, 8\pi^{3/2} \, L^2/(N_o \cdot (1+k^2L^2)^{3/2} \cdot k\theta) \qquad (1)$$

where N_o is the background ionospheric density, ΔN is the density variation, L is the outer scale size parameter, and k is the irregularity wavenumber. Woodman and Basu used Eq. (1) to test whether Jicamarca radar irregularity data (50 MHz frequency, 3 m scale size) obey the power law distribution previously found to be valid for experimental, in-situ, hectometer sized irregularity data. Using their assumed values of $N = 6\times10^{11}/m^3$, $(\overline{\Delta N})^2 = 36\times10^{20}/m^3$, and L = 20 km, which are compatible with the present data, and ALTAIR parameters of $k_{VHF} = 6.3\ m^{-1}$, $k_{UHF} = 17\ m^{-1}$, $\theta_{VHF} = 0.047$ radian, and $\theta_{UHF} = 0.019$ radian, yields P_{hF}/P_{hI} (VHF) = 53 dB and P_{hF}/P_{hI} (UHF) = 40 dB. The measured ALTAIR results at UHF are 3 to 6 dB below the value obtained from Eq. (1) and the VHF results are 6 to 8 dB less than Eq. (1) numbers. Closer agreement with the measured value at either one of the frequencies can be obtained by reasonable adjustment of the L or the $(\overline{\Delta N})^2$ parameters. However, in that case, a 3 dB discrepancy still occurs at the remaining frequency.

A direct determination of the spectral slope in the 1 to 3/8 m regime can be made from the ALTAIR VHF and UHF data themselves without resort to additional assumptions. The ratio of measured

VHF to UHF quasi-coherent signals, normalized to a common illuminated volume, is 10.5 $\pm$ 2.5 dB. Thus, the slope of the log of the power spectral curve versus the log of the wavenumber in this region is -2.4 $\pm$ 0.6. Assuming a generalized power law spectrum

$$P_{hF}(UHF)/P_{hF}(VHF) \propto \left[\frac{k_{UHF}}{k_{VHF}}\right]^{-m} \qquad (2)$$

where m = 2.4 $\pm$ 0.6. Since these results refer to a two dimensional process, they imply that the empirical one dimensional power spectrum $\propto k^{-n}$, where n = 1.4 $\pm$ 0.6 in this region. Thus, the empirically determined slope of the power spectrum for irregularity sizes between 1 and 3/8 m is somewhat shallower than indicated by the power law index of m = 3 from Eq. (1) for intermediate sized irregularities. These results suggest that a process of irregularity cascading from larger to smaller sizes is also operative in the submeter region. An abrupt cut-off of irregularity formation for sizes below the ion gyro-radius previously anticipated by Woodman and Basu is ruled out by the present data except during the decay phase. A possible explanation of the occurrence of irregularities in this domain is given by Huba et al. (1978). Although the present results indicate that the spectral index is somewhat smaller in the submeter region than it is in the intermediate irregularity size region, they do not test whether a power law spectrum is valid in the submeter region. In combination with Woodman and Basu's results, it appears that a transition region from one cascading process to another occurs in the vicinity of the 3 m irregularity size.

B. Irregularity Decay and Associated Scintillation

The ALTAIR measurements of 11 August 1978 during the decay phase of backscatter echoes uncovered several interesting facts. The 3/8 m irregularities decayed very shortly before the 1 m irregularities. As the small scale irregularities decayed, a

larger scale sized depleted plasma region appeared in their stead. After the decay of the meter sized irregularities, the depleted plasma regions continued to exist for at least a short interval unaccompanied by the meter sized irregularities. Scintillation measurements were made on the WIDEBAND SATELLITE which passed over the depleted region during this period and strong scintillations were observed.

On at least a dozen separate occasions during this series, scintillations of transiting satellite echoes were observed to occur, without exception, in the same regions in which quasi-coherent backscatter signals were detected by ALTAIR. Conversely, when satellite scintillations were observed in the geomagnetic orthogonality regions, they were found to be accompanied by quasi-coherent backscatter signals with the exception of the above described situation on 11 August 1978. The implication is that the presence of quasi-coherent backscatter signals is a positive indication of the coexistence of larger, scintillation associated irregularities. Furthermore, the existence of scintillation sized irregularities appears to indicate the coexistence of small scale irregularities except during the decay phase of the scintillation.

C. Plasma Bubble Models

The cause of the formation of generalized Spread-F in the equatorial ionosphere has long eluded ionospheric investigators. The current most widely held theory (Scannapieco, A. and S. Ossakow, August 1976; Woodman, R. and C. LaHoz, 1976; and Ossakow, S. et al., April 1978) portrays a Rayleigh Taylor instability on the F-region bottomside as leading to a plasma depleted region, or plasma bubble, which subsequently rises through the F-region layer causing small scale irregularity formation on its sides and in its wake. The measurements reported here show conclusive evidence of plasma depleted regions. However, these measurements indicate that the plasma depletions were

associated with the decay of the fine scale irregularities instead of their formation. It is possible, although it presently appears unlikely, that plasma bubbles occurred in the middle of the F-region during the formative stage of the irregularity development on 11 August 1978, which were not detected by ALTAIR. Variations in the thickness of the F-region layer, extending hundreds of km horizontally observed by the radar during the irregularity formation stage, did not appear to be associated with mid-layer plasma bubbles. In comparing the results of this set of measurements with model predictions, it should be kept in mind that these measurements represent specific observations for a particular set of conditions which may or may not be typical of the general morphology. The bottomside altitude history observations described above, which indicate a growth of echo regions when the bottomside was rising above 300 km and a decay in echoes when the bottomside was falling below 250 km, appear consistent with plasma bubble model predictions. A large amount of ALTAIR data regarding the behavior of the ionospheric background and the small scale irregularities remains to be analyzed and correlated with other observations and calculations.

REFERENCES

1. "Wideband Equatorial Program," SDC-TM-1290K, Space Data Corporation (March 1978).
2. Woodman, R. and S. Basu, "Comparison Between In-Situ Spectral Measurements of F-Region Irregularities and Backscatter Observations at 3-m Wavelength," Geophys. Res. Lett. 5, 869 (1978).
3. Huba, J. D., P. K. Chaturvedi, S. L. Ossakow, and D. M. Towle, "High Frequency Drift Waves with Wavelengths Below the Ion Gyro-radius in Equatorial Spread-F," Geophys. Res. Lett. 5, 695 (1978).
4. Scannapieco, A. and S. Ossakow, "Nonlinear Equatorial Spread F," Geophys. Res. Lett. 3, 695 (1976).
5. Woodman, R. and C. LaHoz, "Radar Observations of F-Region Equatorial Irregularities," J. Geophys. Res. 81, 5447 (1976).
6. Ossakow, S., et al., "Nonlinear Equatorial Spread F: Dependence on Altitude of the F-Peak and Bottomside Background Electron Density Gradient Scale Length," NRL Memo Rep. 3772, Naval Research Laboratory, Washington, D.C. (April 1978).

APPENDIX A

ELECTRON DENSITY DERIVATION FROM ALTAIR SIGNAL AND CALIBRATION RECORDS

For convenience in measuring the radar cross section of various objects, the gain of the ALTAIR receiver is calibrated to provide a constant output signal from a constant cross section point target independent of its range from the radar. Thus, the output background noise increases as R^4, where R is the radar sample range. Moreover, the radar calibration indicates the RMS system noise output in dB relative to one square meter is xs_{no} = 40LOG(R/R_o) dBsm, where for the 40 usec UHF CW pulse, R_o = 5650 km. Any additional signal, due to incoherent scatter echoes, for example, is measured relative to (i.e., in addition to, in terms of dB) this background noise level.

The Thompson radar cross section of a single electron in a plasma is

$$xs_e = 10^{-28}/(1+T_e/T_i) \ (m^2)$$

where T_e is the electron temperature and T_i is the ion temperature of the plasma. After sunset, the equilibrium electron temperature, T_e, declines to the ion temperature, t_i. Since no independent measurement of this temperature was made during this series and since it approaches unity at nighttime, the approximation for the results presented in this report was made that, $xs_e = 0.5 \times 10^{-28}$ m^2. Errors due to this approximation are expected to be negligible for post sunset data.

The resultant cross section (xs_t) from incoherent scatter from all of the electrons in a given range cell across the antenna beam is

$$xs_t = (R\theta)^2 L \cdot n_e \cdot xs_e \cdot \pi/4 \ (m^2)$$

where L is the pulse length, R is the sample range, and θ is the antenna beamwidth. $\theta^2 \simeq 4\pi/G$, where G is the antenna gain. Therefore, the observed ratio of the incoherent scatter signal to the signal noise background corresponds to

$$xs_t/xs_{no} = \pi^2 \cdot L \cdot xs_e \cdot R_o^4 \cdot n_e/G \cdot R^2$$

In terms of the calibrated cross section signal, S, in dBsm, and the background noise cross section, $10LOGxs_{no}$, in dBsm

$$S - 40LOG\ R/R_o = \delta S = 10LOG(xs_t/xs_{no})$$

and,

$$n_e = G \cdot R^2 \cdot (10^{\delta S/10}-1)/\pi^2 R_o^4 xs_e L\ (m^{-3})$$

Therefore, the electron density is determined directly from the recorded radar cross section signals and the calibration constants. If accurate electron density measurements were also to be made during the daytime, the ratio T_e/T_i would need to be determined by measuring the Doppler characteristics of the incoherent backscatter signal.

UNCLASSIFIED

SECURITY CLASSIFICATION OF THIS PAGE *(When Data Entered)*

REPORT DOCUMENTATION PAGE		READ INSTRUCTIONS BEFORE COMPLETING FORM
1. REPORT NUMBER ESD-TR-79-223	2. GOVT ACCESSION NO.	3. RECIPIENT'S CATALOG NUMBER
4. TITLE *(and Subtitle)* ALTAIR Observations of Ionospheric Irregularities and Background Densities		5. TYPE OF REPORT & PERIOD COVERED *Technical Note* 6. PERFORMING ORG. REPORT NUMBER Technical Note 1979-41
7. AUTHOR(s) David M. Towle		8. CONTRACT OR GRANT NUMBER(s) F19628-78-C-0002
9. PERFORMING ORGANIZATION NAME AND ADDRESS Lincoln Laboratory, M.I.T. P.O. Box 73 Lexington, MA 02173		10. PROGRAM ELEMENT, PROJECT, TASK AREA & WORK UNIT NUMBERS
11. CONTROLLING OFFICE NAME AND ADDRESS Defense Nuclear Agency Hybla Valley Federal Building 6801 Telegraph Road Alexandria, VA 20305		12. REPORT DATE 19 September 1979 13. NUMBER OF PAGES 68
14. MONITORING AGENCY NAME & ADDRESS *(if different from Controlling Office)* Electronic Systems Division Hanscom AFB Bedford, MA 01731		15. SECURITY CLASS. *(of this report)* Unclassified 15a. DECLASSIFICATION DOWNGRADING SCHEDULE

16. DISTRIBUTION STATEMENT *(of this Report)*

Approved for public release; distribution unlimited.

17. DISTRIBUTION STATEMENT *(of the abstract entered in Block 20, if different from Report)*

18. SUPPLEMENTARY NOTES

None

19. KEY WORDS *(Continue on reverse side if necessary and identify by block number)*

ionospheric irregularities
radar scintillation
ionospheric plumes
plasma depleted regions
ALTAIR
equatorial ionosphere

20. ABSTRACT *(Continue on reverse side if necessary and identify by block number)*

A series of measurements of the properties of equatorial ionospheric irregularities were made at Kwajalein, M.I. in August 1977 and July-August 1978. These measurements, ~~sponsored by the Defense Nuclear Agency (DNA)~~, involved coordinated ground based and in-situ sensors. The ARPA Long-range Tracking and Instrumentation Radar (ALTAIR), ~~operated by Lincoln Laboratory,~~ obtained backscatter and transmission data during five nights in August 1977 and eight nights in July-August 1978. This report describes the ALTAIR data from the night of 11 August 1978 which yield direct quantitative measurements of 1 m and 3/8 m irregularities and of plasma depleted regions. These plasma depleted regions, previously predicted on the basis of theoretical speculation and in-situ data, appear to be associated with the decay phase and not the generative phase of the field aligned irregularities.

DD FORM 1 JAN 73 1473 EDITION OF 1 NOV 65 IS OBSOLETE

UNCLASSIFIED

SECURITY CLASSIFICATION OF THIS PAGE *(When Data Entered)*